Astronomy & Astrophysics manuscript no. Paper˙final
February 3, 2012

On the molecular gas content and SFR in Hickson Compact Groups: enhanced or deficient?⋆

V. Martinez-Badenes[1], U. Lisenfeld[2], D. Espada[1,3], L. Verdes-Montenegro[1], S. García-Burillo[4], S. Leon[5], J. Sulentic[1], and M. S. Yun[6]

[1] Instituto de Astrofísica de Andalucía (IAA/CSIC), Apdo. 3004, 18080, Granada, Spain. e-mail: vicentm@iaa.es,
[2] Departamento de Física Teórica y del Cosmos, Facultad de Ciencias, Universidad de Granada, Spain. e-mail: ute@ugr.es,
[3] National Astronomical Observatory of Japan, 2-21-1, Osawa, Mitaka, Tokyo 181-8588, Japan
[4] Observatorio Astronómico Nacional (OAN) Observatorio de Madrid, C/ Alfonso XII 3, 28014, Madrid, Spain
[5] Joint ALMA Observatory/ESO, Vitacura, Santiago, Chile.
[6] Department of Astronomy, University of Massachusetts, Amherst, MA 01003, USA.

Preprint online version: February 3, 2012

ABSTRACT

Aims. We study the effect of the extreme environment in Hickson Compact groups (HCGs) on the molecular gas mass, M_{H_2}, and the star formation rate (SFR) of galaxies as a function of atomic hydrogen (HI) content and evolutionary phase of the group.
Methods. We have selected a redshift limited (D<100 Mpc) sample of 88 galaxies in 20 HCGs with available atomic hydrogen (HI) VLA maps, covering a wide range of HI deficiencies and evolutionary phases of the groups, and containing at least one spiral galaxy. We derived the far-infrared (FIR) luminosity (L_{FIR}) from IRAS data and used it as a tracer of the star formation rate (SFR). We calculated the HI mass (M_{HI}), L_{FIR} and M_{H_2} deficiencies.
Results. The mean deficiencies of L_{FIR} and M_{H_2} of spiral galaxies in HCGs are close to 0, indicating that their average SFR and molecular gas content are similar to those of isolated galaxies. However, there are indications of an excess in M_{H_2} ($\sim 50\%$) in spiral galaxies in HCGs which can be interpreted, assuming that there is no systematic difference in the CO-to-H_2 conversion factor, as either an enhanced molecular gas content or as a higher concentration of the molecular component towards the center in comparison to galaxies in lower density environments. In contrast, the mean M_{HI} of spiral galaxies in HCGs is only 12% of the expected value. The specific star formation rate (sSFR= SFR/stellar mass) tends to be lower for galaxies with a higher M_{H_2} or M_{HI} deficiency. This trend is not seen for the star formation efficiency (SFE=SFR/M_{H_2}), which is very similar to isolated galaxies. We found tentative indications for an enhancement of M_{H_2} in spiral galaxies in HCGs in an early evolutionary phase and a decrease in later phases.
We suggest that this might be due to an enhancement of the conversion from atomic to molecular gas due to on-going tidal interactions in an early evolutionary phase, followed by HI stripping and a decrease of the molecular gas content because of lack of replenishment.
Conclusions. The properties of M_{H_2} and L_{FIR} in galaxies in HCGs are surprisingly similar to those of isolated galaxies, in spite of the much higher def(M_{HI}) of the former. The trends of the sSFR and def(M_{H_2}) with def(M_{HI}) and the evolutionary state indicate, however, that the ongoing interaction might have some effect on the molecular gas and SF.

Key words. Galaxies: evolution – Galaxies: groups – Galaxies: interactions – Galaxies: ISM – Galaxies: star formation – ISM: molecules

1. Introduction

Hickson Compact Groups (HCGs) (Hickson 1982) are dense and relatively isolated groups of 4-8 galaxies in the nearby universe. The combination of high galaxy density (Hickson 1982) and low density environment coupled with low systemic velocity dispersions ($< \sigma > = 200$ km s^{-1}, Hickson et al. 1992) make HCGs especially interesting systems to study how gas content and star formation activity in galaxies are influenced by the environment.

The most remarkable effect of multiple and strong interactions between galaxies in HCGs involves an atomic gas (HI) deficiency. VLA measures of individual spiral galaxies in HCGs show them to have only 24% of the atomic hydrogen (HI) mass, M_{HI}, expected from their optical luminosities and morphological types (Verdes-Montenegro et al. 2001). The inferred deficiency becomes even larger if one assumes that many of the lenticular galaxies, that are over-represented in HCGs, are stripped spirals. Verdes-Montenegro et al. (2001) proposed an evolutionary sequence for HCGs in which the HI is continuously removed from the galaxies, finally leading to groups where most of the HI is located outside of the galaxies. However, not only the individual galaxies in HCGs are HI deficient, but also HCGs as a whole (Verdes-Montenegro et al. 2001). This leads to the still open question of where the missing HI has gone and by which mechanism it was removed. In order to investigate the role played by a hot intragroup medium (IGM), Rasmussen et al. (2008) performed Chandra and XMM-Newton observations to study eight of the most HI deficient HCGs. They found bright X-ray emission in only 4 groups suggesting that galaxy-IGM interactions are not the dominant mechanism driving cold gas out of the galaxies. Borthakur et al. (2010) found with new single-dish Green Bank Telescope (GBT) observation of HGCs an important diffuse, low-column density intragroup HI component, missed by VLA observations. Taking into account these compo-

⋆ Full Tables 1, 2, 3 and 5 are available in electronic form at the CDS via anonymous ftp to cdsarc.u-strasbg.fr (130.79.128.5) or via http://cdsweb.u-strasbg.fr/cgi-bin/qcat?J/A+A/vvv/ppp and from http://amiga.iaa.es/.

nents reduced, but not completely eliminated, the HI-deficiency of the groups.

The effect of an extreme environment on molecular gas properties is controversial. An enhancement of molecular gas content with respect to isolated galaxies has been reported for strongly interacting systems (Casasola et al. 2004, and references therein), defined in that work as galaxies appearing to be clearly interacting with nearby objects, presenting tidal tails or bridges, merging systems and galaxies with disturbed structures. With respect to galaxies in clusters, no deficiency of the molecular gas content has been found in global studies of the Virgo cluster (Kenney & Young 1986; Boselli et al. 2002) and the Coma Supercluster (Casoli et al. 1991; Boselli et al. 1997) in spite of large HI deficiencies that some galaxies presented. The spatially resolved study of Fumagalli et al. (2009) found, however, that a significant number ($\sim$ 40%) of HI-deficient spiral galaxies was also depleted in molecular gas, *if* the HI was removed from within the optical disk. Scott et al. (in prep.) found a trend for spirals in Abell 1367 in more evolved evolutionary states to be more depleted in $M_{\rm H_2}$ than those in less evolved evolutionary states. Thus, there are indications that the cluster environment does affect the molecular gas content.

For galaxies in HCGs, observations of the molecular gas up to date are inconclusive. Leon et al. (1998) found the $M_{\rm H_2}/L_{\rm B}$ ratio of galaxies in HCGs to be enhanced with respect to a sample of field and interacting galaxies. On the contrary, Verdes-Montenegro et al. (1998) found no evidence for an enhancement of the molecular gas mass ($M_{\rm H_2}$) in HCG galaxies relative to a sample of isolated galaxies. Studying the relation between atomic and molecular gas for a sample of 32 spiral galaxies, Verdes-Montenegro et al. (2001) found tentative evidence for a depressed molecular gas content in HI deficient galaxies in HCGs.

The level of star formation (SF) in HCGs has also been subject to considerable debate with original claims of a far-infrared (FIR) excess (Hickson et al. 1989) subsequently challenged (Sulentic & de Mello Rabaca 1993). From the enhanced SF observed in galaxy pairs (Xu & Sulentic 1991), an increase in SF in HCGs might be expected as a consequence of the continuous encounters and tidal interactions which take place within such groups. Nevertheless, the Star Formation Rate (SFR) in HCGs, obtained from FIR (Verdes-Montenegro et al. 1998), mid-infrared (Bitsakis et al. 2010) and Hα luminosities (Iglesias-Páramo & Vílchez 1999) has been found to be similar to those of the control samples.

There have been a few attempts to study the relation of $M_{\rm H_2}$ and $L_{\rm FIR}$ with the HI properties of the HCG galaxies. Verdes-Montenegro et al. (2007), based on CO, FIR and HI single-dish data, together with VLA maps for 8 groups, found that the $M_{\rm H_2}$ and $L_{\rm FIR}$ are lower than expected for HI deficient galaxies, when compared to a well-defined sample of isolated galaxies (AMIGA project, Analysis of the interstellar Medium of Isolated GAlaxies, http://amiga.iaa.es; Verdes-Montenegro et al. 2005). A possible explanation for this trend is that, as HI is needed to replenish the molecular clouds and molecular gas is necessary to fuel SF, a HI deficiency ultimately can lead to a decrease in the SFR. However, the result of Verdes-Montenegro et al. (2007) was based on a small sample of galaxies that does not cover the wide range of properties of HCGs and was therefore not statistically significant. On the other hand, while previous works studying $M_{\rm H_2}$ and SFR of galaxies in HCGs (Verdes-Montenegro et al. 1998; Leon et al. 1998) were based on larger samples, those did not have the HI mass of the individual galaxies to compare with $M_{\rm H_2}$ and $L_{\rm FIR}$. Thus, up to date, no study of the relation between $M_{\rm H_2}$, $M_{\rm HI}$ and SFR for a statistically significant sample has been carried out.

To shed light on the relations between $M_{\rm H_2}$ and SFR with $M_{\rm HI}$ properties of the HCGs, we present here a systematic study for galaxies in a sample of 20 HCGs for which we have HI measurements for the entire groups, as well as for a large fraction of the individual galaxies. This enables us to take into account $M_{\rm HI}$ of the galaxies as an additional parameter, as well as the evolutionary phase of the group according to Verdes-Montenegro et al. (2001) (see Sect. 2). We compare the properties of galaxies in HCGs with those of isolated galaxies in the AMIGA sample (Verdes-Montenegro et al. 2005). Our goal is to determine whether deviations in the HI content with respect to isolated galaxies translate into anomalies in the $M_{\rm H_2}$ and the SFR.

The outline of this paper is as follows. We present the sample in Sec. 2. CO(1-0) and CO(2-1) data coming either from our observations or from the literature, together with reprocessed IRAS FIR data, are presented in Sec. 3. In Sec. 4 we compare the $M_{\rm H_2}$, $L_{\rm FIR}$ (as a tracer of the SFR) and $M_{\rm HI}$ of the galaxies, studying their deficiencies and their relation with the HI content and evolutionary phase of the group. A discussion of a possible evolutionary sequence for the molecular gas content in the HCGs is presented in Sec. 5. Finally, the conclusions of our work are summarized in Sec. 6.

2. The Samples

2.1. Galaxies in HCGs

Our sample was selected from the revision of the original Hickson (1982) catalogue performed by Hickson et al. (1992). From the groups included in that work, we study 86 galaxies belonging to 20 different HCGs: 7, 10, 15, 16, 23, 25, 30, 31, 37, 40, 44, 58, 67, 68, 79, 88, 92, 93, 97 and 100. The groups, which cover all evolutionary stages and a wide range of HI deficiencies, satisfy the following criteria:

- Having at least four members, so triplets are excluded, according to the original Hickson (1982) criterion. We also exclude false groups, where a single knotty irregular galaxy has been confused with separated galaxies (Verdes-Montenegro et al. 2001).
- Containing at least one spiral galaxy, since we are mainly interested in studying the relation between the SF process and $M_{\rm H_2}$, which are most clearly linked for spiral galaxies.
- Being at a distance $D \leq$100 Mpc (assuming H_0=75 km s^{-1} Mpc^{-1}), so that observations of groups have a better sensitivity limit and minimize possible source confusion within the telescope beam. At 100 Mpc, the 30m beam would have a size of 10.7 kpc and the VLA beam (considering a size of 50″×50″) 24.2 kpc.

The HCGs in our sample cover the full range of HI contents. Their deviation from normalcy is measured with respect to that of isolated galaxies, as given by Haynes & Giovanelli (1984). This deviation is usually referred to as deficiency and is defined as the decimal logarithm of the ratio between the sum of the expected HI masses for all the galaxies in the group, based on their optical luminosity and morphology, and the HI mass of the entire group as derived from the single dish observations in Borthakur et al. (2010) (see Verdes-Montenegro et al. 2001, and also Sec. 4.2). As a function of their total HI deficiency, the HCGs in our sample can be classified as follows:

– HCGs with a normal HI content (at least 2/3 of its expected value): HCG 23, 25, 68 and 79.
– HCGs with a slight HI deficiency (between 2/3 and 1/3 of the expected value): HCG 7, 10, 15, 16, 31, 37, 40, 58, 88, 92, 97 and 100.
– HCGs with a large HI deficiency (under 1/3 of the expected value): HCG 30, 44, 67 and 93.

Verdes-Montenegro et al. (2001) proposed an evolutionary sequence model where the HI is continuously stripped from the galaxies. According to this model, HCGs can be classified into 3 phases as follows: in Phase 1 the HI is mainly found in the disks of galaxies. In Phase 2, 30% to 60% of the HI has been removed from the disks by tidal interaction. Finally, in Phase 3, almost all the HI is found out of the galactic disks, either forming tidal tails of stripped gas (Phase 3a) or, in a few cases, in a large HI cloud with a single velocity gradient in which the galaxies are embedded (Phase 3b).

According to the evolutionary phases defined in Verdes-Montenegro et al. (2001), the HCGs in our sample were classified by Borthakur et al. (2010) as:

– Phase 1: HCG 7, 23, 67, 79 and 88.
– Phase 2: HCG 10, 16, 25, 31, 40[1] , 58 and 100.
– Phase 3: HCG 15, 30, 37, 44, 68, 92, 93 and 97.

The evolutionary state is an indicator of the evolution of the cold ISM of the group but it does not necessarily give the age of the group. E.g. HCG79 consists on 3 early-type galaxies and one intruding spiral galaxy. Stellar halo data indicates that it is an old group (Durbala et al. 2008). However, since the main part of the HI is located within the disk of the intruder galaxy, it is classified in evolutionary phase 1.

We revised the velocities of the individual galaxies in the HCGs of our sample. Two galaxies not considered in Hickson et al. (1992) have been added: HCG100d, which had no velocity data in that work, and HCG31g, added to the catalogue of HCGs by Rubin et al. (1990).

The basic properties of the galaxies in our sample are detailed in Table 1. The columns are:

1. Galaxy: galaxy designation, following the notation of Hickson (1982).
2. V: heliocentric radial velocity in km s^{-1}(weighted average of optical measurements taken from the LEDA[2] database) converted from the optical to the radio definition for comparison with the CO spectra.
3. σ_V: velocity dispersion of the galaxies in the group.
4. D: distance to the corresponding HCG in Mpc, derived from the mean heliocentric velocity of the group as D = V/H$_0$, assuming a value of H$_0$ = 75 km s^{-1} Mpc^{-1}. The mean velocity of the group is calculated averaging the velocity of the individual galaxies (column 2).
5. T: morphological type taken from LEDA, following the RC3 classification (de Vaucouleurs et al. 1991).
6. D_{25}: optical major diameter in arcmin at the 25 mag arcsec^{-2} isophot taken from LEDA.
7. B_c^T: apparent blue magnitude taken from LEDA, corrected for Galactic dust extinction, internal extinction and K-correction.
8. log(L_B): decimal logarithm of the blue luminosity, derived from B_c^T as:

$$\log\left(\frac{L_B}{L_\odot}\right) = 2\log D - 0.4B_c^T + 11.95. \quad (1)$$

   This definition provides an estimate of the blue luminosity (νL_ν) at 4400 Å.
9. log(L_K): decimal logarithm of the luminosity in the K-band in units of the solar luminosity in the K_S-band ($L_{K,\odot}$ = 5.0735×10^{32} erg s^{-1}), calculated from the extrapolated magnitude in the K_S (2.17 μm) band from the 2MASS Extended Source Catalogue (Jarrett et al. 2000). We calculated the K_S luminosity, L_K, from the total (extrapolated) K_S flux, f_K, as $L_K = \nu f_K(\nu)$ (where ν is the frequency of the K-band, 1.38×10^{14} Hz) .
10. log(M_{HI}): logarithm of the mass of the atomic hydrogen, in solar masses, for 66 of the galaxies in our sample observed with the VLA, using different combinations of the C and D configurations with beam sizes ranging from 16″×14″ to 72″×59″ (Verdes-Montenegro et al. 2001, and Verdes-Montenegro, private communication).

2.2. Reference sample: Isolated galaxies

We chose the AMIGA sample of isolated galaxies (Verdes-Montenegro et al. 2005), which is based on the CIG catalogue (Karachentseva 1973), as a reference for the FIR and molecular gas properties. The FIR properties of an optically complete subsample of this catalogue have been studied in Lisenfeld et al. (2007). The data that we are using for this subsample are slightly different from Lisenfeld et al. (2007) because we have taken into account a recent update of some basic properties which affects the blue magnitude, distance, morphological type and isolation degree (detailed information are provided in Fernández-Lorenzo 2011). We also use the CO data of a velocity restricted subsample (1500<V<5000 km s^{-1}) of 173 AMIGA galaxies (Lisenfeld et al. 2011) to compare to our galaxies. For the analysis of the HI properties we use the work of Haynes & Giovanelli (1984), presenting the observations and analysis of CIG galaxies, as a reference.

There are two intrinsic differences between the AMIGA and the HCG samples that must be taken into account when performing a comparison: (i) the HCG sample has a larger rate of early-type galaxies (~45%), whereas 87% of the AMIGA galaxies are spirals (Fig. 1) and (ii) the sample of AMIGA galaxies with M_{H_2} data is restricted to a velocity range of 1500< V <5000 km s^{-1}, while the range of the HCGs extends to larger velocities. Thus, the isolated galaxies are, on average, at a lower distance (47 Mpc average distance versus 68 Mpc for the HCG sample) which can explain their lower average luminosities (see Table 6). However, the values of the deficiencies, ratios or correlations, that we are going to discuss in the following are not expected to be affected by the difference in distance.

3. The data

3.1. CO data

We obtained CO data, either by our observations or from the literature, for 86 galaxies in the selected 20 HCGs. CO data are missing for only 2 galaxies in these 20 groups, HCG 67d and HCG 92f. The CO(1-0) line was detected for 45 galaxies.

[1] While HCG 40 was classified in Verdes-Montenegro et al. (2001) as Phase 3, new VLA observations (Yun et al. in preparation) showed that a significant amount of HI was missed due to a narrow spectral window, and based on these data has been reclassified as Phase 2.

[2] http://leda.univ-lyon1.fr/intro.html

Table 1. Basic parameters of the galaxies in the HCG sample

Galaxy	V	σ_V	D	T(RC3)	D_{25}	B_c^I	$\log(L_B)$	$\log(L_K)$	$\log(M_{HI})$
	(km s^{-1})	(km s^{-1})	(Mpc)		(arcmin)	(mag)	($L_\odot$)	($L_\odot$)	($M_\odot$)
(1)	(2)	(3)	(4)	(5)	(6)	(7)	(8)	(9)	(10)
7a	4141	117	53.4	1.0	2.06	12.96	10.22	11.09	9.12
7b	4175	117	53.4	-1.9	1.27	14.29	9.69	10.78	<7.83
7c	4347	117	53.4	5.0	1.71	13.36	10.06	10.80	9.56
7d	4083	117	53.4	-1.4	0.94	14.04	9.79	10.11	9.00
10a	5104	269	65.6	3.1	2.92	12.53	10.57	11.27	...
....	....	....	....	....	....	....	....	....	....

Notes. The full table is available in electronic form at the CDS and from http://amiga.iaa.es.

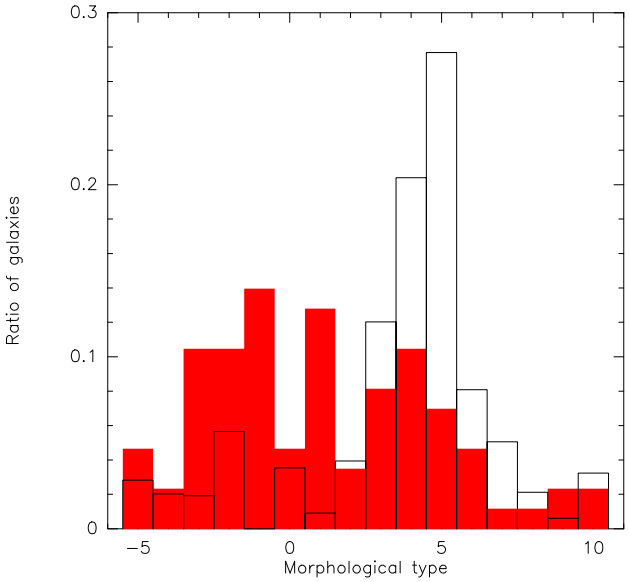

Fig. 1. Morphological types, T(RC3), for the AMIGA isolated (black line) and HCGs (red filled bars) galaxies.

3.1.1. IRAM CO(1-0) and CO(2-1) observations and data reduction

We observed 47 galaxies belonging to 14 different HCGs. The observations of the CO rotational transition lines J=1→0 and J=2→1 (at 115.271 and 230.538 GHz, respectively) were carried out with the IRAM 30m radio telescope at Pico Veleta[3] during June, October and December 2006. We performed single-pointing observations using the wobbler switch mode, with a switch frequency of 0.5 Hz and a throw of 200″. We checked for all the objects that the off-position did not coincide with a neighbor galaxy.

The dual polarization receivers A100 and B100 were used to observe in parallel the CO(1-0) and CO(2-1) lines. The median system temperature was 231 K for the CO(1-0) observations, with ∼80% of the galaxies observed with system temperatures between 150 and 350 K. In the case of CO(2-1), the median system temperature was 400 K, with a temperature range between 230 and 800 K for 85% of the galaxies. For CO(1-0) the 1 MHz filterbank was used, and for CO(2-1) the 4 MHz filterbank. The corresponding velocity resolutions were 2.6 km s^{-1} and 5.3 km s^{-1} for CO(1-0) and CO(2-1), respectively. The total bandwidth was 1 GHz. The Half Power Beam Width (HPBW) is 22″ and 11″ for 115 and 230 GHz, respectively. All CO spectra and intensities are presented on the main beam temperature scale (T_{mb}) which is defined as $T_{mb} = (F_{eff}/B_{eff}) \times T_A^*$. The IRAM forward efficiency, F_{eff}, was 0.95 and 0.91 at 115 and 230 GHz, and the beam efficiency, B_{eff}, was 0.75 and 0.54, respectively.

The data reduction and analysis was performed using CLASS, while further analysis was performed using GREG, both part of the GILDAS[4] package developed by IRAM. First we visually inspected the spectra and discarded bad scans. Then, spikes were removed and a constant or linear baseline was subtracted from each spectrum. The scans were then averaged to achieve a single spectrum for each galaxy and transition. These spectra were smoothed to a velocity resolution of 21 to 27 km s^{-1}, depending on the rms. A total of 24 galaxies were detected in CO(1-0) (2 of them marginal), 22 in CO(2-1) (4 of them marginal) and 18 in both transitions. The spectra are shown in Appendix A, Fig. A.1 displays the spectra detected in CO(1-0) and Fig. A.2 those detected in CO(2-1).

For each spectrum, we integrated the intensity along the velocity interval where emission was detected. In the case of non-detections we set an upper limit as:

$$I_{CO} < 3 \times rms \times \sqrt{\delta V\ \Delta V}, \quad (2)$$

where δV is the channel width and ΔV is the total line width. We used a value of ΔV = 300 km s^{-1} when there was no detection in CO(1-0) or CO(2-1). In those cases where the source was detected in only one transition, this line width was used to calculate the upper limit in the other transition.

The results of our CO(1-0) and CO(2-1) observations are displayed in Table 2. The columns are:

1. Galaxy: galaxy designation.
2. $I_{CO(1-0)}$: velocity integrated intensity of the CO(1-0) emission in K km s^{-1}.
3. rms : root-mean-square noise of the CO(1-0) spectrum (if available) in mK.
4. Ref.: reference of the CO(1-0) data, detailing whether data come from our observations or from the literature (see 3.1.2).
5. Beam: HPBW of the telescope in arc second.
6. $\Delta V_{CO(1-0)}$: line width of the CO(1-0) emission (if detected) in km s^{-1}.
7. $I_{CO(2-1)}$: velocity integrated intensity of the CO(2-1) emission (if observed) in K km s^{-1}.
8. rms: rms of the CO(2-1) spectrum (if observed) in mK.
9. $\Delta V_{CO(2-1)}$: line width of the CO(2-1) emission (if detected) in km s^{-1}.
10. $\log(M_{H_2\ obs})$: logarithm of the H_2 mass (in solar masses) calculated from the observed central I_{CO} (see Sec.3.1.3).
11. $\log(M_{H_2})$: logarithm of the H_2 mass (in solar masses) extrapolated to the emission from the total disk (see Sec. 3.1.3).

[3] IRAM is supported by CNRS/INSU (France), the MPG (Germany) and the IGN (Spain).

[4] http://www.iram.fr/IRAMFR/GILDAS

Table 2. Observed and derived molecular gas properties

Galaxy	$I_{CO(1-0)}$ (K km s^{-1})	rms (mK)	Ref.	HPBW (arcsec)	ΔV (km s^{-1})	$I_{CO(2-1)}$ (K km s^{-1})	rms (mK)	ΔV (km s^{-1})	log($M_{H_2 obs}$) ($M_\odot$)	log(M_{H_2}) ($M_\odot$)
(1)	(2)	(3)	(4)	(5)	(6)	(7)	(8)	(9)	(10)	(11)
7a	7.20		3	43	500				9.51	9.71
7b	< 0.70		3	55	...				<8.71	<8.80
7c	1.40		3	55	183				9.01	9.17
7d	< 0.60		3	43	...				<8.43	<8.52
10a	2.72±0.49		2	22	339				8.79	9.51
....	....	....	....	....	....	....	....	....	....	....

(1)CO reference: 1: Our observations. 2: Leon et al. (1998). 3: Verdes-Montenegro et al. (1998).
Notes. The full table is available in electronic form at the CDS and from http://amiga.iaa.es.

3.1.2. CO(1-0) data from the literature

We have searched in the literature for available CO(1-0) data for the 20 HCGs of our sample and have compiled data for the velocity integrated CO(1-0) intensities and line widths (also listed in Tab. 2) from the following sources:

- Verdes-Montenegro et al. (1998): 24 galaxies from 9 different HCGs. 20 of these galaxies were observed with the NRAO 12 m telescope at Kitt Peak with a beam size of 55″. The data from the other 4 galaxies are from Boselli et al. (1996), observed with the SEST 15m telescope, with a 43″ beam. Two of these galaxies (68d and 88c) were also observed by us, but we chose the Verdes-Montenegro et al. (1998) data because of their better quality.
- Leon et al. (1998): 17 galaxies corresponding to 10 different HCGs, observed with the IRAM 30m telescope with a similar setting as in our observations (see Sec. 3.1.1).

There are 16 galaxies that were observed both by us and by Verdes-Montenegro et al. (1998) or Leon et al. (1998). Furthermore, 14 galaxies were observed by both Verdes-Montenegro et al. (1998) and Leon et al. (1998). In order to choose between the different existing spectra (either from our observations or from the literature), we first checked that they were consistent and then applied the following criteria: if available, we chose the spectrum with detected emission. If more than one detected spectrum existed, we chose the one with the lower rms or –in case of comparable rms- the spectrum observed with a larger beam, in order to probe a larger fraction of the disk. Except for the two galaxies mentioned above, we always selected our data due to their better quality in case of duplication. In total, we have CO(1-0) spectra for 86 galaxies (45 from our own observations and 41 from the literature) for our statistical analysis.

3.1.3. Molecular gas mass

We calculate the molecular gas mass, M_{H_2} using the following equation:

$$M_{H_2} = 75 \times D^2 I_{CO(1-0)} \Omega \quad (3)$$

where Ω is the area covered by the observations in arcsec^2 (i.e. $\Omega = 1.13\ \theta^2$ for a single pointing with a gaussian beam where θ is the HPBW). This equation assumes a CO-to-H_2 conversion factor X=$N_{H_2}/I_{CO} = 2 \times 10^{20}$cm^{-2} (K km s^{-1})$^{-1}$ (e.g. Dickman et al. 1986). No correction factor for the fraction of helium and other heavy metals is included. The molecular gas masses of the AMIGA galaxies are calculated in the same way.

In both the observations that we carried out and the data from the literature, a single position at the center of the galaxy was observed. Because of this and the different beams used by us and in the literature we need to correct for possible emission outside the beam. To extrapolate the observed CO intensities to the total value within the disk we need to know the distribution and extension of the CO emission. Different authors (Nishiyama et al. 2001; Regan et al. 2001; Leroy et al. 2008) found that the velocity integrated CO intensity in spiral galaxies follows an exponential distribution as a function of radius with a scale length r_e:

$$I_{CO}(r) = I_0 \propto \exp(r/r_e) \quad (4)$$

We adopt a scale length of $r_e = 0.2 \times r_{25}$, where r_{25} is the major optical 25 mag arcsec^{-2} isophotal radius, following Lisenfeld et al. (2011), who derive this scale length from studies of the mentioned authors and from their own CO data. We have used this distribution to calculate the expected CO emission from the entire disk, taking into account the galaxy inclination (see Lisenfeld et al. 2011, for more details). This approach assumes that the distribution of the molecular gas in galaxies in HCGs is the same as in field spiral galaxies. The implications of this approach will be discussed.

The resulting aperture correction factor for M_{H_2} (defined as the ratio between M_{H_2} observed in the central pointing and M_{H_2} extrapolated to the entire disk) is shown in Figure 2. The ratio between the extrapolated and central intensities is below 2 for most galaxies (66 out of 86, or 77%), with an average value of 1.78. To check the consistency of the extrapolation, we have also performed the analysis presented in this paper for a sample restricted to galaxies with a small (less than a factor 1.6) aperture correction ($n = 45$), finding no significant differences with

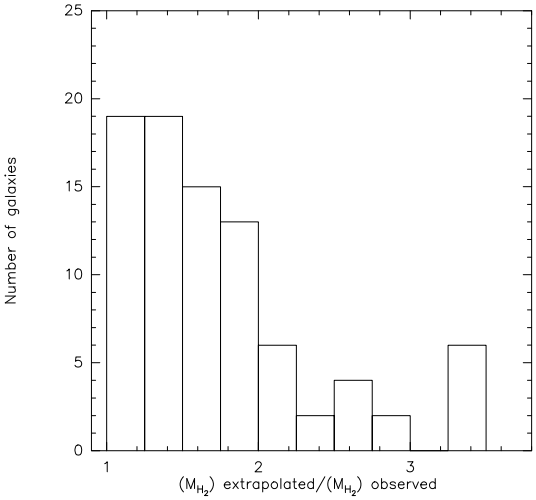

Fig. 2. Distribution of the aperture correction factor for M_{H_2}.

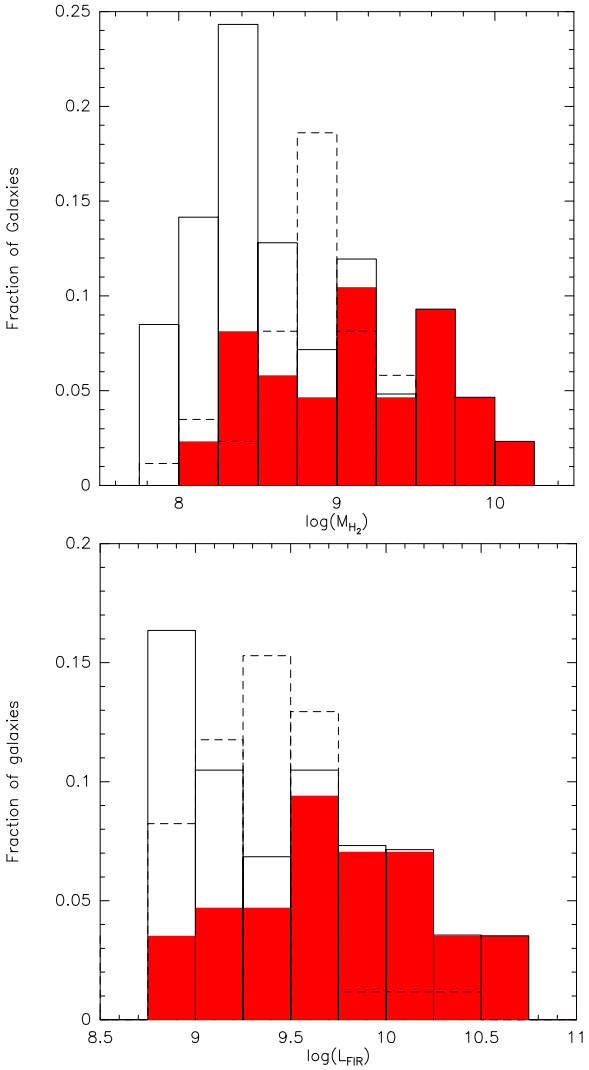

Fig. 3. $M_{\rm H_2}$ and $L_{\rm FIR}$ distribution of the HCG galaxies. The red filled bins show the distribution of the detected galaxies, the dashed line gives the distribution of upper limits and the full line shows the distribution calculated with ASURV.

respect to the full sample. Thus, we conclude that the aperture correction does not introduce any bias in the results.

The values for the molecular gas mass in the central pointing and the extrapolated molecular gas mass are listed in Table 2. Here, and in the following, we always use the extrapolated molecular gas mass and denote it as $M_{\rm H_2}$ for simplicity. The $M_{\rm H_2}$ distribution is shown in Fig. 3. The average value for spiral galaxies ($T \geq 1$) is listed in Table 6. The distribution and average values of $M_{\rm H_2}$, as well as the statistical distributions and average values throughout this work, have been calculated using the Kaplan-Meier estimator implemented in ASURV[5], to take into account the upper limits in the data.

3.2. Far-Infrared Data

FIR fluxes were obtained from ADDSCAN/SCANPI, a utility provided by the Infrared Processing and Analysis Center (IPAC)[6]. This is a one-dimensional tool that coadds calibrated survey data of the Infrared Astronomical Satellite (IRAS). It makes use of all scans that passed over a specific position and produces a scan profile along the average scan direction. It is 3-5 times more sensitive than the IRAS Point Source Catalog (PSC) since it combines all survey data and it is therefore more suitable for detection of the total flux from slightly extended objects.

We have compiled from Verdes-Montenegro et al. (1998) the FIR data (also derived using ADDSCAN/SCANPI) for 63 galaxies in our sample. In the case of the remaining 23 galaxies, we derived FIR fluxes directly using ADDSCAN/SCANPI. To choose the best flux estimator we have followed the guidelines given in the IPAC website[7], which are also detailed in Lisenfeld et al. (2007). As a consistency check, we also applied this procedure to 14 galaxies in the list of Verdes-Montenegro et al. (1998). We found no significant differences, with an average difference of 15% between our reprocessed fluxes and those in Verdes-Montenegro et al. (1998).

From the fluxes at 60 and 100 μm the FIR luminosity, $L_{\rm FIR}$, is computed as:

$$\log(L_{\rm FIR}/L_{\odot}) = \log(FIR) + 2\log(D) + 19.495 \quad (5)$$

where FIR is defined as (Helou et al. 1988):

$$FIR = 1.26 \times 10^{-14}(2.58\,F_{60} + F_{100}){\rm Wm}^{-2}. \quad (6)$$

The computed $L_{\rm FIR}$, together with the 60 and 100 μm fluxes compiled from ADDSCAN/SCANPI, are detailed in Table 3. The distribution of $L_{\rm FIR}$ is shown in Fig. 3. The average value of $L_{\rm FIR}$ for spiral galaxies is given in Table 6.

For galaxies HCG 31a and HCG 31c the FIR fluxes could not be separated. Therefore, we use the sum of both. When comparing $L_{\rm FIR}$ to other magnitudes ($L_{\rm B}$, $M_{\rm H_2}$ or M_{HI}), we also use the sum of both galaxies.

In order to check the accuracy of the low resolution IRAS data, we compared them to 24μm data from Spitzer for the 12 groups for which Spitzer data is available. We compared the SFR derived from $L_{\rm FIR}$ (calculated from eq. 10) to that derived from the Spitzer 24μm luminosity, $L_{24\mu{\rm m}}$, (from Bitsakis et al. 2010, 2011) using the equation $SFR(M_{\odot}{\rm yr}^{-1}) = 8.10 \times 10^{-37}(L_{24\mu{\rm m}}({\rm erg\,s}^{-1}))^{0.848}$ (from Calzetti et al. 2010). For most of the objects the agreement was satisfactory: the values of the SFR derived in both ways agreed to better than a factor 2.5 or, in case of IRAS upper limits, the resulting upper limits for the SFR were above those derived from $L_{24\mu{\rm m}}$. There were only 3 galaxies in 2 groups with a larger discrepancy: for HCG 79b and for HCG 37b we obtained a value of the SFR derived from IRAS that was a factor of 6 higher than the SFR from the 24μm data and for HCG 37a the difference was a factor of 10. After checking the Spitzer images and IRAS data, we found that in the case of HCG 79 the reason for the discrepancy was the blending of HCG 79a and 79b in the IRAS beam. We thus assumed that the value of $L_{\rm FIR}$ given for HCG 79b in Verdes-Montenegro et al. (1998) arises from both galaxies and assigned to each object a fraction of the IRAS fluxes and $L_{\rm FIR}$ such that SFR(IRAS)=SFR(24μm). A similar situation occurred in the case of HCG 37, where 3 objects (HCG 37a, HCG 37b and HCG 37c) are blended in the IRAS beam. Here, we assume that the value of $L_{\rm FIR}$ given for HCG 37b in Verdes-Montenegro et al. (1998) was emitted from all three galaxies and correctedin the same way as for HCG 79.

[5] Astronomical Survival Analysis (ASURV) Rev. 1.1 (Lavalley et al. 1992) is a generalised statistical package that implements the methods presented by Feigelson & Nelson (1985)

[6] http://scanpi.ipac.caltech.edu:9000/

[7] http://irsa.ipac.caltech.edu/IRASdocs/scanpi_interp.html

Table 3. FIR, SFR, SFE and sSFR

Galaxy	Ref[(1)]	I_{60} (Jy)	I_{100} (Jy)	log(L_{FIR}) ($L_\odot$)	SFR ($M_\odot$ yr^{-1})	log(SFE)[(2)] (yr^{-1})	log(sSFR) ($M_\odot$ yr^{-1})
7a	2	3.32	6.61	10.23	3.75	-9.14	-10.33
7b	2	< 0.18	< 0.32	< 8.95	<0.20		<-11.30
7c	2	0.61	2.35	9.65	0.99	-9.18	-10.62
7d	2	< 0.15	< 0.39	< 8.95	<0.20		<-10.63
10a	2	0.50	1.81	9.72	1.16	-9.45	-11.02
....	....	....	....	....	....	....	....

(1) Reference code (see 3.2): 1: Our data analysis. 2: Verdes-Montenegro et al. (1998).
(2)The value of the SFE is not displayed for the galaxies with upper limits in both L_{FIR} and M_{H_2}.
Notes. The full table is available in electronic form at the CDS and from http://amiga.iaa.es.

4. Results

In this section, we aim to study the relation between M_{H_2} and the SFR in HCG galaxies and compare them to isolated galaxies. Furthermore, we search for relations with the atomic gas deficiency of the galaxies and the groups and with the evolutionary phase of the groups. We furthermore investigate the ratio between the two CO transitions, CO(1-0) and CO(2-1).

In order to search for differences to isolated galaxies, we used two methods: (i) We normalized M_{H_2} and L_{FIR} to the blue luminosity, L_B, or the luminosity in the K-band, L_K, and compared the ratios to those of isolated galaxies, and (ii) we calculated the deficiency parameters of M_{H_2}, L_{FIR} and M_{HI} of the galaxies (see Sect. 4.2). We obtained in general very consistent results for L_B and L_K.

We carry out this analysis separately for early-type galaxies and spirals because of the following reasons: (i) the morphological distribution is very different for both samples, with a much larger fraction of early-type galaxies among HCG galaxies, (ii) the number of early-type galaxies in the AMIGA reference sample is very small so that no statistically significant comparison sample is available. In particular, no deficiency parameter can be derived. (iii) Early-type galaxies tend to have a significantly lower molecular gas content than late-type galaxies, and their FIR emission is not as clearly related to their SFR as it is in late-type galaxies, as a result of the lack of strong SF. Therefore, the use of L_{FIR} as a SF tracer is more questionable.

4.1. Relation between M_{H_2}, L_{FIR}, M_{HI} and L_B

Fig. 4 shows M_{H_2} (top) and L_{FIR} (bottom) versus L_B for spirals galaxies (left) and early-type galaxies (right). For spiral galaxies good correlations exist between both M_{H_2}, respectively L_{FIR}, and L_B. A linear fit to the total sample of HGCs is plotted, together with the corresponding fit to the AMIGA sample. The coefficients are listed in Table 4. A slightly shift towards higher values in M_{H_2} seems to be present in comparison to the best-fit line of isolated galaxies. The linear regressions between L_{FIR} and L_B, M_{H_2} and L_B or M_{H_2} and L_{FIR} (Table 4) show no significative differences between HCGs and isolated galaxies. For early-type galaxies no clear correlation is visible and for log(L_B) $\gtrsim$ 10, the values of both M_{H_2} and L_{FIR} are below those of spiral galaxies.

We note that, in contrast to M_{H_2} and L_{FIR}, M_{HI} shows no correlation with L_B (Fig. 5) reflecting the fact that HI is very strongly affected by the interactions and in many galaxies of our evolved groups largely removed from the galaxies.

Previous surveys (see e.g. Young & Scoville 1991) have found a linear correlation between M_{H_2} and L_{FIR}. A linear correlation can also be seen in our sample (Fig. 6). We include in this figure the lines for constant L_{FIR}/M_{H_2} values equal to 1, 10 and 100 $L_\odot/M_\odot$. Practically all of our galaxies lie in the range of $L_{FIR}/M_{H_2} = 1-10\,L_\odot/M_\odot$, typical for normal, quiescent galaxies (Young & Scoville 1991).

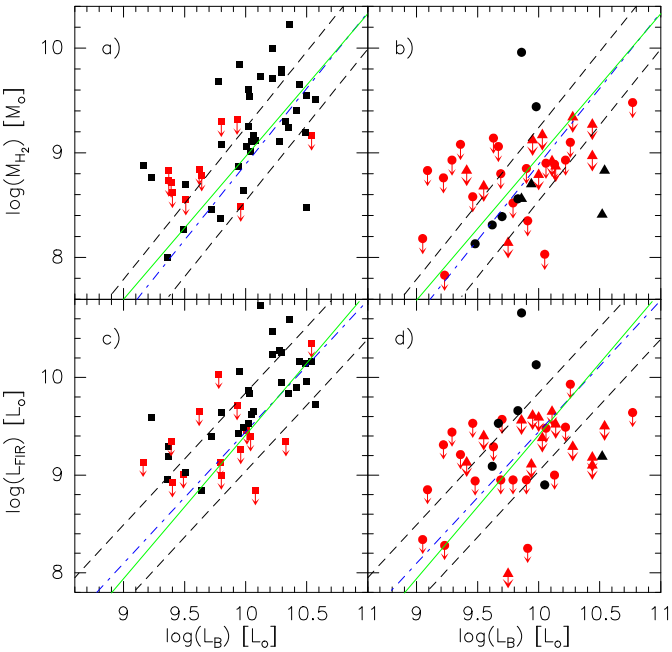

Fig. 4. M_{H_2} vs L_B for *a)* spiral galaxies (T≥1) and *b)* elliptical (circles) and S0 galaxies (triangles). L_{FIR} vs L_B for *c)* spiral galaxies (T≥1) and *d)* elliptical (circles) and S0 galaxies (triangles). The full green line corresponds to the bisector fit found for HCG galaxies (fit parameters are given in Table 4), while the blue dashed-dotted line corresponds to the bisector fit found for the AMIGA isolated galaxies. Both fits are done for the entire range of morphological types. The dashed black lines are offset by the standard deviation of the correlation for the isolated galaxies, which is ±0.35 for the M_{H_2} and ±0.4 for L_{FIR}. Black symbols denote detections and red symbols upper limits.

Finally, we have directly compared E and S0 galaxies in HCGs to galaxies of the same types in the AMIGA sample. In the case of lenticular galaxies we have limited the sample in HCGs to the same distance range as the AMIGA sample (40 - 70 Mpc) since for the largest distances the rate of upper limits is very high in HCGs and does not provide any further information. In Fig. 7 (top) we show the relation between M_{H_2} and L_B for the S0s in HCGs and from the AMIGA sample. Even though the number of data points is low, a trend seems to be present for S0s in isolated galaxies to have a higher M_{H_2} for the same L_B. A similar result is found for L_{FIR} (not shown here), where

Table 4. Correlation analysis of M_{H_2} vs L_B, L_{FIR} vs L_B and M_{H_2} vs L_{FIR}

Magnitude	Sample		Slope (bisector)	Intercept (bisector)	Slope (L_B indep.)	Intercept (L_B indep.)
M_{H_2} vs L_B	HCGs	All	1.37±0.15	-4.74±1.48	0.81±0.14	0.73±1.35
		T>0	1.40±0.16	-4.94±1.61	0.95±0.20	-0.43±1.97
	AMIGA		1.45±0.08	-5.61±0.77	1.12±0.08	-2.43±0.83
L_{FIR} vs L_B	HCGs	All	1.47±0.16	-5.29±1.54	0.79±0.15	1.43±1.49
		T>0	1.31±0.16	-3.37±1.99	0.77±0.16	2.00±1.58
	AMIGA		1.35±0.04	-4.06±0.37	1.12±0.04	-1.73±0.38
M_{H_2} vs L_{FIR}	HCGs	All	0.90±0.09	0.41±0.83	0.75±0.09	1.82±0.86
		T>0	1.21±0.11	-2.63±1.11	1.04±0.11	-1.00±1.08
	AMIGA		1.16±0.08	-2.14±0.72	0.98±0.06	-0.46±0.61

The slope and intercept are defined as $\log(M_{H_2}) = \log(L_B) \times slope$ + intercept, $\log(L_{FIR}) = \log(L_B) \times slope$ + intercept and $\log(M_{H_2}) = \log(L_{FIR}) \times slope$ + intercept. The fits on L_{FIR} vs L_B for the AMIGA sample are slightly different from the values in Lisenfeld et al. (2007) because we have taken into account a recent update of the basic properties of the galaxies (e.g. distance and morphological type; see Fernández-Lorenzo 2011, for more details). The AMIGA fits involving M_{H_2} are taken from Lisenfeld et al. (2011).

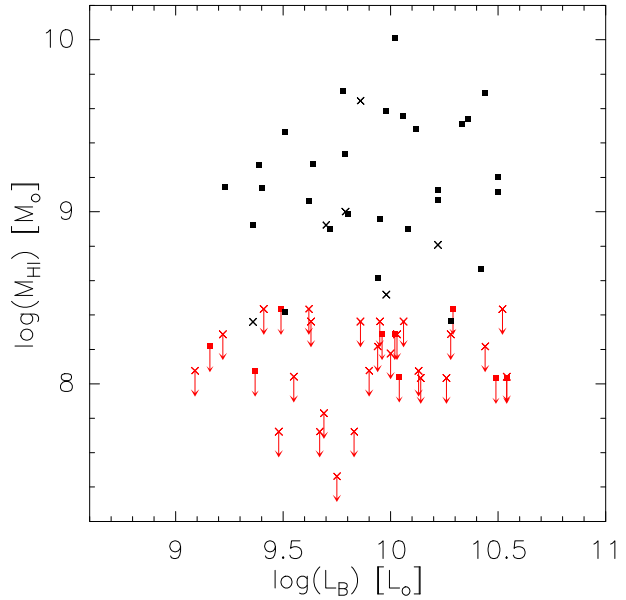

Fig. 5. M_{HI} vs L_B for late-type (T≥1, squares) and early-type (crosses) galaxies. Black symbols denote detections and red symbols upper limits.

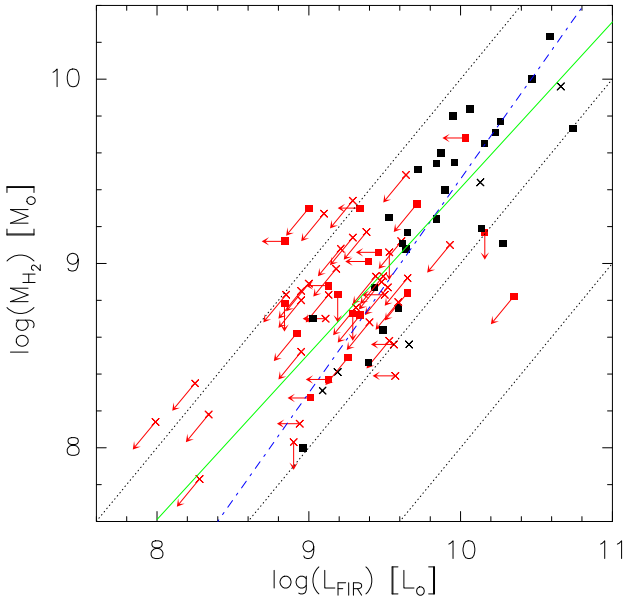

Fig. 6. M_{H_2} vs L_{FIR} for late-type (T≥1, squares) and early-type (E+S0, crosses) galaxies. The green line corresponds to the bisector fit found for HCGs galaxies, while the blue dashed-dotted line corresponds to the bisector fit found for the AMIGA isolated galaxies from Lisenfeld et al. (2011). The fits are detailed in Table 4. The dotted black lines correspond to the L_{FIR}/M_{H_2} ratios 1 (left), 10 (middle) and 100 (right) $L_\odot/M_\odot$. Black symbols denote detections and red symbols upper limits.

most lenticular isolated galaxies present higher values than expected for their optical luminosity, while most of the objects in HCGs show upper limits excluding any excess. If S0 galaxies in these dense environments originate from stripping of spirals, this might indicate that molecular gas has also been removed in the process. Although this interpretation is speculative due to the low statistics, it provides hints for further research in future works.

Concerning the elliptical galaxies, none of the isolated galaxies is detected in CO, while among the four detections in HCGs two have a mass similar to the expected for spiral isolated galaxies (HCG 15d and HCG 79b) while the other two show significantly lower masses (HCG 37a and HCG 93a), pointing to an external origin (Fig. 7, bottom). The FIR luminosity of the Es in HCGs (not shown here) is similar to that expected for spiral galaxies. It is also noticeable that while the range of L_B values for the S0s in HCGs covers about the same range as for isolated galaxies, Es in HCGs are up to half an order of magnitude more luminous than isolated Es.

4.2. Deficiencies

We have calculated the M_{H_2}, L_{FIR} and M_{HI} deficiencies following the definition of Haynes & Giovanelli (1984) as

$$\mathrm{Def}(X) = \log(\mathrm{X_{predicted}}) - \log(\mathrm{X_{observed}}) \quad (7)$$

where we calculated the predicted value of the variable X from L_B. Following this definition, a negative deficiency implies an excess with respect to the predicted value.

The expected M_{H_2} for each galaxy is calculated from its L_B using the fit to the AMIGA sample in Lisenfeld et al. (2011). Note that the fit, which is given in Table 4, was calculated without distinguishing morphological types. Due to the dominance of spiral galaxies in the AMIGA sample, the fit is only adequate for spiral galaxies. Because of the low number of early-type galaxies in the AMIGA sample it is not possible to derive a

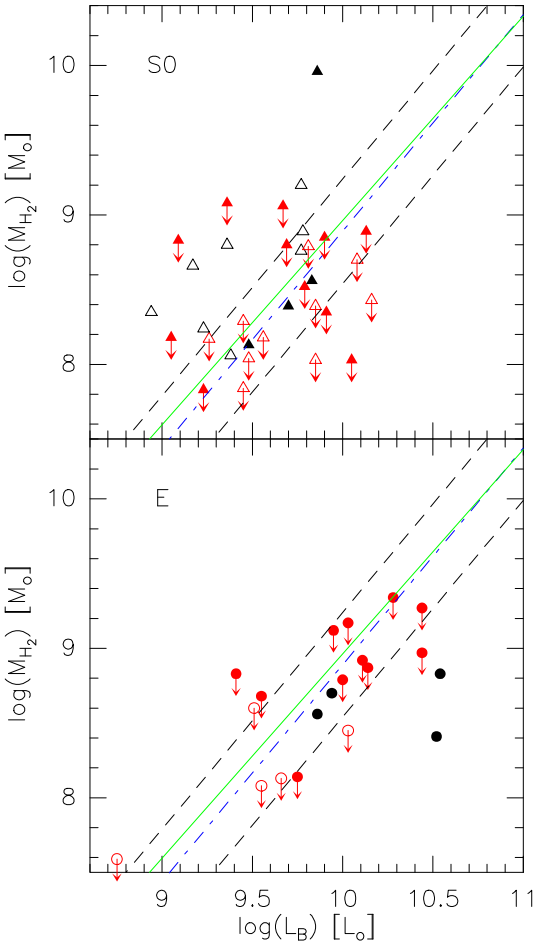

Fig. 7. M_{H_2} vs L_B for early-type galaxies in HCGs (full symbols) and from the AMIGA sample of isolated galaxies (open symbols) with distances between 20 and 70 Mpc. The lines are the same as in Fig. 5a and b. Black symbols denote detections and red symbols upper limits. *Top:* S0 galaxies (triangles), *Bottom:* elliptical galaxies (circles).

meaningful deficiency parameter for them. In addition, we calculated the deficiency derived from the relation between M_{H_2} and L_K of the AMIGA sample (Lisenfeld et al. 2011), $\log(M_{H_2}) = -2.27+1.05\times \log(L_K)$). In a similar way, the expected L_{FIR} is calculated from the fit between L_{FIR} and L_B obtained for the AMIGA isolated galaxies (Table 4) for the sample presented in Lisenfeld et al. (2007).

The correlations between M_{H_2} (respectively L_{FIR}) and L_B, or L_K, have a considerable scatter with standard deviations of 0.35 dex for M_{H_2} and 0.4 dex for L_{FIR}. These standard deviations are much higher than the observational measurement errors. In this case, the error of the mean values are completely dominated by the statistical errors and therefore we neglect the observational errors in our calculations. The high standard deviation means that individual galaxies with deficiencies up to about these values can just represent normal deviations from the mean. However, the much smaller error of the *mean* deficiency allows to compare samples of galaxies (here: galaxies in HCGs and isolated galaxies) with a higher precision.

The HI deficiency of the galaxies is calculated following the morphology-dependent fit between M_{HI} and L_B in Haynes & Giovanelli (1984). We have considered h = H_0/100 = 0.75. We adapted their results which were based on mag_{zw} to our use of B_c^T with the relation found by Verdes-Montenegro et al. (2005) ($mag_{zw} = B_c^T+0.136$). Taking furthermore into account that we express L_B as a function of the solar bolometric luminosity (mag = 4.75), we introduce the following correction:

$$(\log L_B)_{Haynes} = (\log L_B)_{ours} + 0.14 \quad (8)$$

to express L_B in the terms we assume (Sec. 2) to calculate the expected content of HI. The deficiencies in M_{H_2}, L_{FIR} and M_{HI} derived from L_B are listed in Table 5.

Table 5. Deficiencies of M_{H_2}, L_{FIR}, and M_{HI} derived from L_B

Galaxy	Def(M_{H_2})	Def(L_{FIR})	Def(M_{HI})
7a	-0.50	-0.49	0.67
7b	>-0.36	>0.07	>1.38
7c	-0.19	-0.13	0.29
7d	>-0.06	>0.21	0.28
10a	0.21	0.49	...
....	....	....	....

Notes. The full table is available in electronic form at the CDS and from http://amiga.iaa.es.

4.2.1. M_{H_2} and L_{FIR} deficiencies

The mean M_{H_2} and L_{FIR} deficiencies for spiral galaxies in HCGs are similar (see Table 6). Galaxies showing an excess in M_{H_2} or L_{FIR} have values spanning over the full range of L_B, as can be seen in Fig. 4. Thus, the excess in M_{H_2} or L_{FIR} is not associated with the brightest objects *per se*. We have checked in detail the properties of the 9 galaxies showing the largest M_{H_2} excess (HCG 10c, HCG 16a, HCG 16c, HCG 16d, HCG 23b, HCG 23d, HCG 40c, HCG 58a, HCG 88c), and we find that half of them present strong signs of distortion (tidal tails in the optical and/or HI, kinematical perturbations, etc).

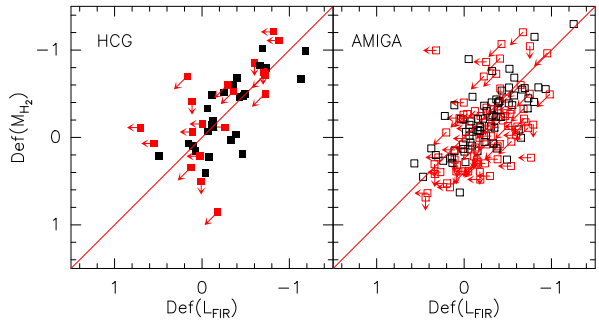

Fig. 8. M_{H_2} deficiency vs L_{FIR} deficiency for late-type (T≥1) galaxies in HCGs (left) and from the AMIGA sample (right). Red symbols represent upper limits in either M_{H_2} or L_{FIR}, and black symbols detections. The y=x line is plotted as reference and does not represent a fit to the data.

Fig. 8 (left) shows Def(M_{H_2}) (from L_B) vs Def(L_{FIR}) for each galaxy. Both are strongly correlated, which can be understood as due to the causal relation between the molecular gas and SFR, leading to a lower SFR if the molecular gas as the fuel for SF decreases. For comparison, Fig. 8 (right) displays Def(M_{H_2}) of the isolated galaxies versus their Def(L_{FIR}). The behavior of the isolated galaxies does not show a significant difference compared to galaxies in HCGs with a very similar range covered by both samples. However, for the isolated galaxies, Def(M_{H_2}) extends to

Table 6. Mean values for spiral galaxies ($T \geq 1$) in HCGs and from the AMIGA sample. The mean values and their errors are calculated with ASURV, taking upper limits into account. We neglect observational errors since the data is dominated by statistical errors. The quoted errors represent the error of the mean values, not the standard deviation.

	HCGs		**AMIGA**[(1)]	
	Mean	n_{UL}/n	Mean	n_{UL}/n
$\log(L_B)$ ($L_\odot$)	9.95±0.06	0/46	9.75±0.04	0/150
$\log(M_{H_2})$ ($M_\odot$)	9.02±0.09	11/46	8.38±0.09	64/150
$\log(L_{FIR})$ ($L_\odot$)	9.53±0.09	15/45	9.16±0.05	58/150
$Def(M_{H_2})$ (from L_B)	-0.14±0.09	11/46	0.06±0.04	64/150
$Def(M_{H_2})$ (from L_K)	-0.15±0.06	10/45	-0.01±0.05	58/149
$Def(L_{FIR})$	-0.11±0.08	15/45	-0.09±0.04	58/150
Def(HI)	0.93±0.13	9/37	-	-
$\log(M_{H_2}/L_B)$, all L_B ($M_\odot/L_\odot$)	-0.96±0.08	11/46	-1.25±0.04	64/150
$\log(M_{H_2}/L_B)$, low L_B[(2)] ($M_\odot/L_\odot$)	-1.04±0.10	10/22	-1.36±0.05	56/103
$\log(M_{H_2}/L_B)$, high L_B[(3)] ($M_\odot/L_\odot$)	-0.88±0.09	1/24	-1.06±0.05	8/47
$\log(M_{H_2}/L_K)$ ($M_\odot/L_{K,\odot}$)	-1.58±0.05	10/45	-1.76±0.05	50/135
$\log(L_{FIR}/L_B)$	-0.45±0.07	15/45	-0.52±0.03	58/149

[(1)]The mean values of the AMIGA galaxies are calculated for the subsample of galaxies with M_{H_2} data. For each subsample, n is the number of galaxies and n_{UL} is the number of upper limits. L_{FIR} and L_B of the AMIGA galaxies are from the new data release (see Sec. 2.2), while M_{H_2} and L_K are from Lisenfeld et al. (2011).
[(2)] for $L_B < 10^{10}\ L_\odot$
[(3)] for $L_B > 10^{10}\ L_\odot$

slightly lower values for a given $Def(L_{FIR})$. This is also reflected in the mean values of $Def(M_{H_2})$ and $Def(L_{FIR})$ of AMIGA and HCG galaxies (Table 6): while the values of $Def(L_{FIR})$ for spiral galaxies are almost the same for both samples, $Def(M_{H_2})$ in spirals is larger by 0.15-0.20 for HCG than for AMIGA galaxies (corresponding to a 40-60% larger M_{H_2} than expected for isolated galaxies).

The histograms shown in Fig. 9 underline these findings: whereas the distribution of $Def(M_{H_2})$ for spiral galaxies in HCGs is shifted to negative deficiencies (i.e. an excess) compared to AMIGA galaxies, the distribution of $Def(L_{FIR})$ is very similar for spiral galaxies in HCGs and in the AMIGA sample. Two sample tests (Gehan's Generalized Wilcoxon Test and Logrank Test) confirm that the distributions of $Def(M_{H_2})$ are different with a probability of $> 96\%$, whereas the distributions $Def(L_{FIR})$ are identical with a non-negligible probability.

As an additional test, we have compared the ratios M_{H_2}/L_B and M_{H_2}/L_K of HCG galaxies to those of isolated galaxies (values are listed in Table 6). In the case of M_{H_2}/L_B we have derived the ratios both for the entire luminosity range and for low ($L_B \leq 10^{10}\ L_\odot$) and high ($L_B > 10^{10}\ L_\odot$) luminosity galaxies in order not to be affected by the nonlinearity of the M_{H_2}-L_B relation. In all cases we found a lower ratio (by $\sim$ 0.2-0.3 dex) for the isolated galaxies, confirming our findings from the deficiency parameter.

The larger M_{H_2} for a given L_B found for spiral galaxies in HGCs could be explained in three ways: a) a real excess of the total molecular gas mass (and will be further discussed as such in the following section), b) a higher concentration towards the center of the molecular gas in HCG galaxies compared to isolated galaxies, so that the extrapolation of the flux based on a similar extent (see Sec. 3.1.3) would lead to an overestimate of M_{H_2}, or c) a systematic difference in the CO-to-H_2 conversion factor between the AMIGA and HCG sample. Although we cannot exclude this possibility, we do not consider it very likely. The CO-to-H_2 conversion factor is known to depend on a number of galactic properties as the metallicity, gas temperture, gas density and velocity dispersion (e.g. Maloney & Black 1988; Narayanan et al. 2011). These properties are likely similar in both samples because of the similar ranges in L_B and L_{FIR} (tracing SFR) that they cover. The first two effects (a and b) could both be at work at the same time. In fact, as indicated in e.g. Leon et al. (2008), galaxies in the AMIGA sample are dominated by disk SF while surveys of compact groups (Menon 1995) show that most radio detections involve compact nuclear emission. This can be explained since nuclear emission is thought to be enhanced by interactions that produce a loss of angular momentum of the molecular gas, that subsequently falls towards the center of the galaxy. These dissipative effects are likely near minimum in isolated galaxies. This result was also proposed by Verdes-Montenegro et al. (1998), where the enhanced I_{25}/I_{100} ratio in HCGs was suggested to be caused by local starbursts, presumably in the nuclear region. This result is still compatible with the conclusion of a normal level of FIR emission among HCG galaxies that we find here, if the activity responsible for enhanced 24μm emission and enhanced/more concentrated molecular gas is localized compared to the overall distribution of gas and dust in the galaxies.

4.2.2. Comparison to the M_{HI} deficiency

In Fig. 10 we display $Def(M_{HI})$ vs $Def(M_{H_2})$ (left) and $Def(L_{FIR})$ (right). The mean value of $Def(M_{HI})$ of the galaxies with available HI data is 0.93 ± 0.13 (12% of the expected value) for spiral galaxies and 1.31 ± 0.11 (5% of the expected value) for all morphological types, which is one order of magnitude larger than $Def(M_{H_2})$ and $Def(L_{FIR})$. We stress here that the samples used in the present paper and in Verdes-Montenegro et al. (2001) are not the same. This earlier study concentrated on the set of data available at that time, which was biased towards HI bright groups. Later, more groups with higher HI deficiencies have been observed with the VLA (Verdes-Montenegro et al. 2007), and are

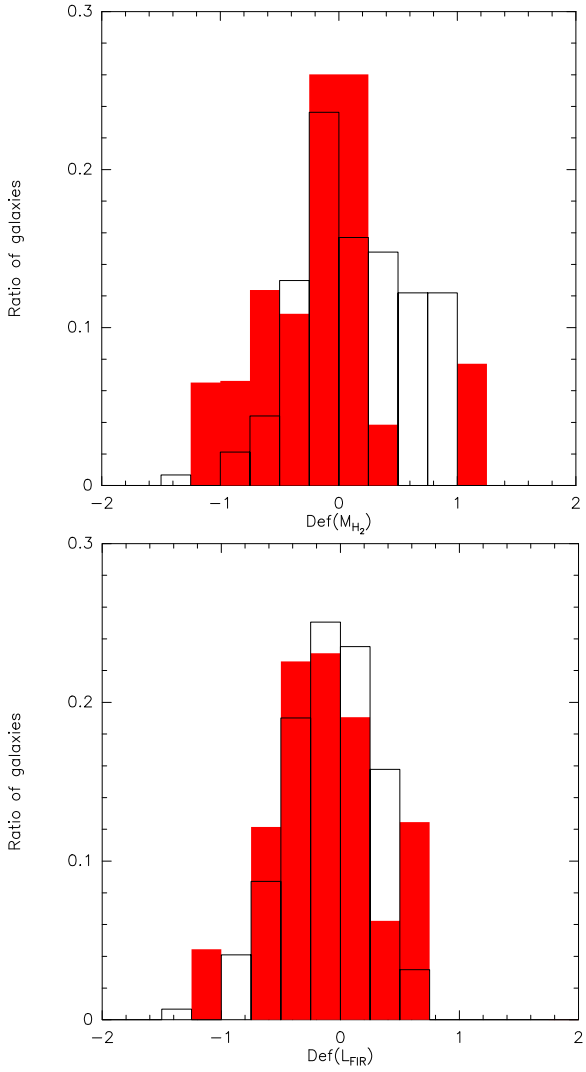

Fig. 9. Def(M_{H_2}) (top) and Def(L_{FIR}) (bottom) distribution of spiral galaxies in AMIGA (black line) and in HCGs (red filled bars), calculated with ASURV in order to take the upper limits into account.

part of the present sample. Therefore, the mean HI deficiency of the galaxies in Verdes-Montenegro et al. (2001) (25% of the expected value for spiral galaxies) is less than the mean HI deficiency of the present sample. We have checked that the HI deficiencies calculated in this paper are consistent with the values for the groups in common with Verdes-Montenegro et al. (2001).

Most noticeable in Fig. 10 is that even very HI-deficient galaxies have a rather normal M_{H_2} or L_{FIR}. There is no clear correlation between Def(M_{HI}) and Def(M_{H_2}) or Def(L_{FIR}). There might be a weak trend in the sense that a larger M_{HI} deficiency leads to larger M_{H_2} and L_{FIR} deficiencies. This trend is also seen when calculating the mean deficiencies and ratios separately for low and highly M_{HI} deficient galaxies, here chosen as galaxies with def(M_{HI}) < 0.75 and def(M_{HI}) > 0.75 in order to obtain two groups of roughly the same size (Table 7). However, the differences are small and fall below significance when changing the separation to def(M_{HI}) = 0.50. Thus, the statistics in our sample is not sufficient to firmly conclude whether this trend is real.

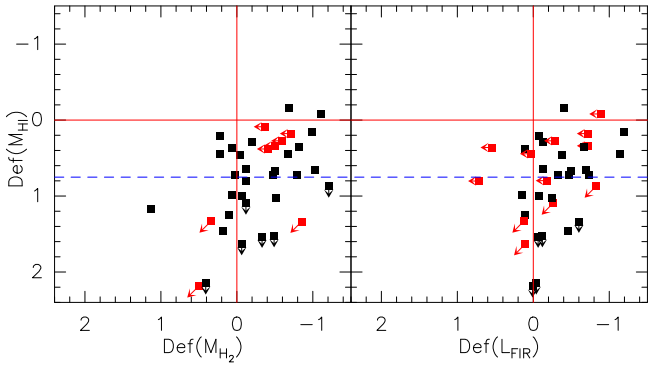

Fig. 10. M_{HI} vs M_{H_2} deficiencies (left) and M_{HI} vs L_{FIR} deficiencies (right) for spiral galaxies (T≥ 1). The red lines show Def(M_{HI}) = 0, Def(M_{H_2}) = 0 and Def(L_{FIR}) = 0, and the dashed lines give Def(M_{H_2})=0.75, separating low and highly HI-deficient galaxies in our analysis. Red symbols denote upper limits in M_{H_2} or L_{FIR}.

4.3. Comparison to the HI content and evolutionary stage of the group

To study the influence of the global HI content of the group on M_{H_2} and SFR of the individual galaxies we have classified the groups as a function of their Def(M_{HI}) as listed in Sec. 2. The average Def(M_{H_2}) and Def(L_{FIR}) of the galaxies belonging to these groups are detailed in Table 7. We find no clear relation between the Def(M_{H_2}) of the galaxies, nor the Def(L_{FIR}), with the global Def(M_{HI}) of the groups.

In a similar way, we calculated the average Def(M_{H_2}) and Def(L_{FIR}) of the galaxies belonging to HCGs in different evolutionary states, as defined by Borthakur et al. (2010) (see Sec. 2), which are also detailed in Table 7. The Def(M_{H_2}) of the galaxies increases slightly as the group evolves along the evolutionary sequence. This trend is also visible in the ratios M_{H_2}/L_B and M_{H_2}/L_K. In the case of Def(L_{FIR}), there is no clear relation for spiral galaxies with the evolutionary state, we only find a trend when considering the total sample, most likely due to a changing fraction of ellipticals.

A very pronounced variation with evolutionary phase is shown by the morphological types (Fig. 11). The ratio of elliptical and S0 galaxies increase strongly in groups in phase 3. It has been proposed (e.g. Verdes-Montenegro et al. 2001; Bekki & Couch 2011) that S0 galaxies in HCGs might be stripped spirals.

4.4. Star Formation Rate, Star Formation Efficiency and specific Star Formation Rate

We calculate the SFR from L_{FIR} following the prescription of Kennicutt (1998):

$$SFR(M_\odot/\mathrm{yr}) = 4.5 \times 10^{-44}\, L_{IR}(\mathrm{ergs}^{-1}) \quad (9)$$

where L_{IR} refers to the IR luminosity integrated over the entire mid- and far-IR spectrum (10-1000 μm). This expression is based on a Salpeter IMF. We convert it to the Kroupa (2001) IMF by dividing by a factor 1.59 (Leroy et al. 2008). In our analysis we use L_{FIR} (eq. 6), which estimates the FIR emission in the wavelength range of 42.5-122.5 μm. We estimate L_{IR} from L_{FIR} using the result of Bell (2003) that on average $L_{IR} \sim 2 \times L_{FIR}$. Taking this into account, we can calculate the SFR from L_{FIR} as:

Table 7. Mean values of deficiencies and ratios of M_{H_2} and L_{FIR} for different samples. Only spiral galaxies (T≥1) are considered. Mean values are calculated as explained in Table 6.

		Def(M_{H_2})	log(M_{H_2}/L_B) ($M_\odot/L_\odot$)	n_{UL}/n	log(M_{H_2}/L_K) ($M_\odot/L_{K,\odot}$)	n_{UL}/n
Total		-0.14±0.09	-0.96±0.08	11/46	-1.58±0.05	10/45
HI content of galaxies	Def(HI)<0.75	-0.34±0.10	-0.82±0.10	5/21	-1.40±0.07	4/20
	Def(HI)>0.75	-0.07±0.16	-1.15±0.13	3/16	-1.77±0.08	3/16
HI content of the group	Normal	-0.38±0.20	-0.76±0.15	1/6	-1.52±0.11	0/5
	Slightly deficient	-0.08±0.11	-0.99±0.10	8/32	-1.59±0.07	8/32
	Very deficient	-0.21±0.08	-0.95±0.10	2/8	-1.60±0.12	2/8
Evolutionary Phase	Phase 1	-0.35±0.14	-0.76±0.11	2/11	-1.46±0.09	1/10
	Phase 2	-0.16±0.13	-0.92±0.12	5/21	-1.55±0.07	5/21
	Phase 3	-0.04±0.09	-1.07±0.08	4/14	-1.71±0.11	4/14
		Def(L_{FIR})	log(L_{FIR}/L_B)	n_{UL}/n	log(L_{FIR}/L_K) ($L_\odot/L_{K,\odot}$)	n_{UL}/n
Total		-0.11±0.08	-0.45±0.07	15/45	-1.14±0.09	14/44
HI content of galaxies	Def(HI)<0.75	-0.32±0.11	-0.28±0.11	6/20	-0.84±0.10	5/19
	Def(HI)>0.75	0.03±0.11	-0.60±0.11	6/16	-1.38±0.13	6/16
HI content of the group	Normal	-0.19±0.19	-0.36±0.11	3/6	-1.07±0.17	2/5
	Slightly deficient	-0.08±0.09	-0.45±0.09	10/31	-1.15±0.11	10/31
	Very deficient	-0.23±0.08	-0.37±0.07	2/8	-1.03±0.14	2/8
Evolutionary Phase	Phase 1	-0.17±0.15	-0.36±0.13	4/11	-1.03±0.13	3/10
	Phase 2	-0.12±0.13	-0.43±0.13	7/20	-1.11±0.14	7/20
	Phase 3	-0.12±0.05	-0.45±0.04	4/14	-1.11±0.09	4/14

For each subsample, n is the number of galaxies and n_{UL} is the number of upper limits.

$$SFR(M_\odot/\mathrm{yr}) = 4.5 \times 2 \times \frac{1}{1.59} \times 10^{-44} L_{FIR}(\mathrm{ergs}^{-1}) = 2.2 \times 10^{-10}\ L_{FIR}(L_\odot) \quad (10)$$

The values of the SFR of the galaxies in our sample are listed in Table 3.

We define the SFE as the ratio between the SFR and the molecular gas mass, SFE = SFR/M_{H_2}. The SFE of the individual galaxies in our sample are listed in Table 3. Fig. 6 shows a good, roughly linear correlation between L_{FIR} and M_{H_2} and indicates that the SFE in our sample is expected to show a rather narrow range. To calculate the average SFE of our sample we must take into account that ASURV can only handle data showing upper or lower limits, but not both. Thus, we have first calculated the average SFE considering only galaxies detected in CO with an upper limit in FIR, together with the ones detected in both bands. Separately, we considered only those detected in FIR but not detected in CO and the ones detected in both bands. The average values are listed in Table 8.

We have calculated the average SFE for the AMIGA sample of isolated galaxies, taking M_{H_2} from Lisenfeld et al. (2011) and L_{FIR} from Lisenfeld et al. (2007), for comparison with the SFE in HCG galaxies. The values are listed in Table 8. We furthermore list the SFE derived from a spatially resolved analysis for 30 nearby galaxies from the HERACLES survey (Bigiel et al. 2011). All values are adjusted to our CO-to-H_2 conversion factor, Kroupa IMF, and no consideration of helium in the molecular gas mass. Tab. 8 shows a slightly lower SFE in HCGs than in AMIGA galaxies, in line with the previous results of an excess in M_{H_2} but a normal value of L_{FIR}. In comparison to the galaxies from the HERACLES survey there is no noticeable difference. Thus, overall there are no strong indications that the process of SF occurs in a different manner in the different environment of HCGs.

The specific SFR, sSFR, is defined as the ratio between the SFR and the stellar mass of a galaxy. We calculated the stellar mass from the K band luminosity since the light in this band is dominated by the emission of low-mass stars, which are responsible for the bulk of stellar mass in galaxies. From L_K we derived the stellar mass, M_*, by adopting a mass-to-luminosity ratio of $M_\odot/L_{K,\odot}$ = 1.32 (Cole et al. 2001) for the Salpeter Initial Mass Function (IMF), and applying a correction factor of 0.5 (from Bell et al. 2003) to change to the Kroupa (2001) IMF used in this paper. The values for the individual galaxies are listed in Table 3. The average sSFR for spiral galaxies in our sample is log(sSFR) =-10.61 ± 0.07 yr^{-1}.

Table 8. Mean log(SFE) for different samples and measurements (only spiral galaxies, T≥1). Mean values are calculated as explained in Table 6.

Sample	<log(SFE) (yr^{-1})>
HCGs	-9.06±0.05[(1)]/-9.22±0.06[(2)]
CIGs	-8.94±0.03[(1)]/-9.07±0.04[(2)]
HERACLES	-9.23[(3)]

[(1)] Values obtained with galaxies detected in both CO and FIR and galaxies detected in FIR but not detected in CO. [(2)] Values obtained with galaxies detected in both CO and FIR and galaxies detected in CO but not detected in FIR. [(3)] from Bigiel et al. (2011). The 1σ standard deviation is 0.24dex.

4.4.1. SFE and sSFR as a function of the deficiencies of the galaxies

In Fig. 12 we display the SFE and the sSFR of the spiral galaxies in our sample as a function of their Def(M_{HI}) and Def(M_{H_2}). There is no clear trend of the SFE with the gas deficiency of the galaxies, neither atomic nor molecular. This is confirmed by the mean values listed in Table 9. This result indicates that SF proceeds with the same efficiency, independently of whether it occurs in a galaxy with a low or high M_{HI} deficiency.

On the other hand, galaxies with a lower def(M_{H_2}) or def(M_{HI}) tend to have a higher sSFR (see Fig.12, as well as

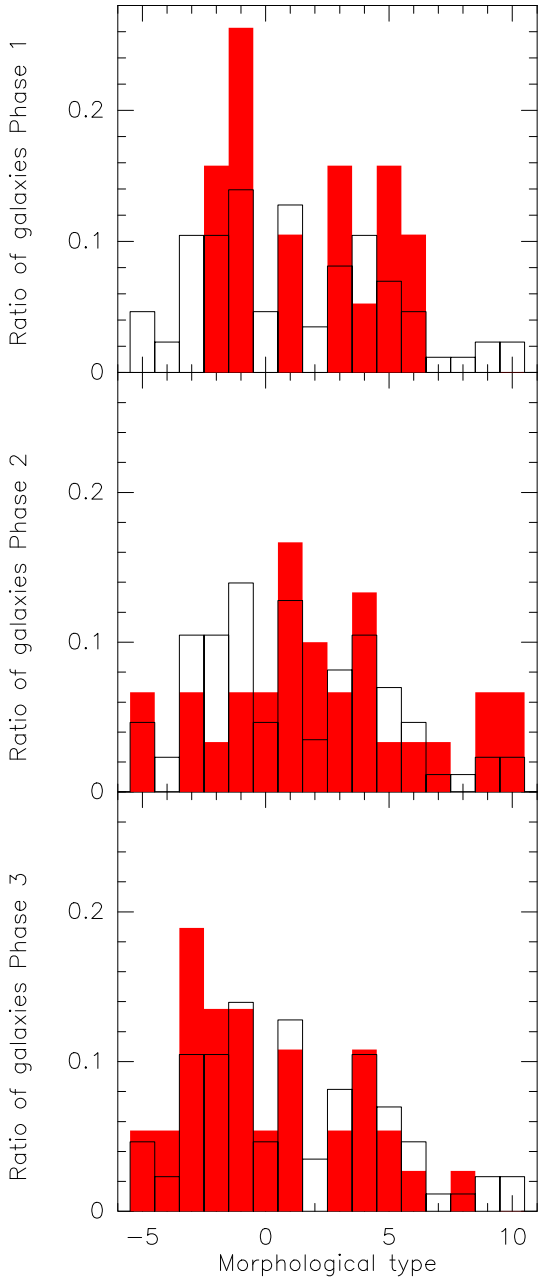

Fig. 11. Morphological type distribution for different evolutionary phases. From top to bottom, the morphological type distribution of galaxies in HCGs in evolutionary phases 1, 2 and 3 are plotted. The filled red bins correspond to the distribution for the groups in each evolutionary state, while the black line bins correspond, for comparison, to galaxies of all phases.

Table 9 for the quantitative trends). In particular, the trend with def($M_{\rm HI}$) is interesting as it suggests that, although the Def($M_{\rm HI}$) of a galaxy has no influence on the absolute SFR or SFE, it has a noticeable effect on the SFR per stellar mass.

4.5. Line Ratio

Fig. 13 shows the CO(1-0) versus the CO(2-1) intensity for the galaxies we observed (Sec. 3.1.1). The plotted intensities are not aperture corrected. The mean ratio between both intensities is $I_{\rm CO(2-1)}/I_{\rm CO(1-0)}$ = 1.13±0.11 for the full sample and 1.13±0.12 for spiral galaxies only. To calculate this mean ratio

Table 9. Mean log(sSFR) and log(SFE) as a function of Def($M_{\rm HI}$) and Def($M_{\rm H_2}$) for spiral galaxies ($T \geq 1$). Mean values are calculated as explained in Table 6.

	log(sSFR)(yr^{-1}) Mean	n_{UL}/n
Def($M_{\rm HI}$) <0.75	-10.31±0.10	(5/19)
Def($M_{\rm HI}$) >0.75	-10.85±0.13	(6/16)
Def($M_{\rm H_2}$) < -0.25	-10.33±0.07	(6/22)
Def($M_{\rm H_2}$) > -0.25	-10.81±0.12	(8/22)
	log(SFE)(yr^{-1}) Mean	n_{UL}/n
Def($M_{\rm HI}$) <0.75	-9.08±0.07	(5/19)
Def($M_{\rm HI}$) >0.75	-9.16±0.12	(6/16)
Def($M_{\rm H_2}$) < -0.25	-9.05±0.07	(6/22)
Def($M_{\rm H_2}$) > -0.25	-9.04±0.13	(8/22)

For each subsample, n is the number of galaxies and n_{UL} is the number of upper limits.

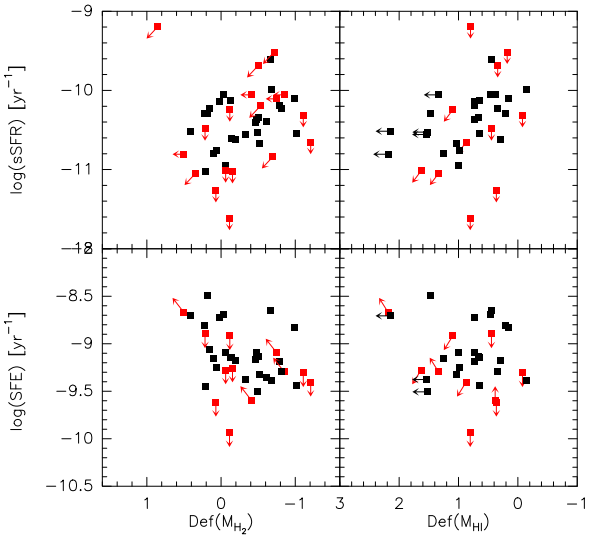

Fig. 12. Specific SFR (sSFR) (top) and star formation efficiency (SFE) (bottom), vs $M_{\rm H_2}$ and $M_{\rm HI}$ deficiencies of spiral galaxies ($T \geq 1$) in HCGs. Red symbols denote upper limits in $M_{\rm H_2}$ or $L_{\rm FIR}$.

with ASURV, we have taken into account galaxies with detections in both CO transitions as well as those detected only in CO(1-0). These values are slightly higher than those found by Leroy et al. (2009) from CO(2-1) and CO(1-0) maps for nearby galaxies from the SINGS sample ($I_{\rm CO(2-1)}/I_{\rm CO(1-0)}$ ~0.8) and than those from Braine et al. (1993) who obtained a mean line ratio of $I_{\rm CO(2-1)}/I_{\rm CO(1-0)}$ = 0.89 ± 0.06 for a sample of nearby spiral galaxies. Both values are, in contrast to ours, corrected for beam-size effects.

In order to interpret the ratio of $I_{\rm CO(2-1)}/I_{\rm CO(1-0)}$ one has to consider two main parameters: the source distribution and the opacity. For optically thick, thermalized emission with a point-like distribution we expect a ratio $I_{\rm CO(2-1)}/I_{\rm CO(1-0)}$ = $(\theta_{CO(1-0)}/\theta_{CO(2-1)})^2 = 4$ (with $I_{\rm CO}$ in $T_{\rm mb}$ and θ being the FWHM of the beams). On the other hand, for a uniform source brightness distribution we expect ratios larger than 1 for optically thin gas, and ratios between about 0.6 and 1 for optically thick gas (with excitation temperatures above 5 K).

Due to the different beam sizes of CO(1-0) and CO(2-1) in our observations we cannot distinguish these two cases. However, we can conclude that our values are consistent with

optically thick, thermalized gas with an extended distribution. Our mean value is slightly higher than the (beam-corrected) values of Leroy et al. (2009) and Braine et al. (1993) which might indicate that the molecular gas is not completely uniform over the CO(1-0) beam, but slightly concentrated towards the center.

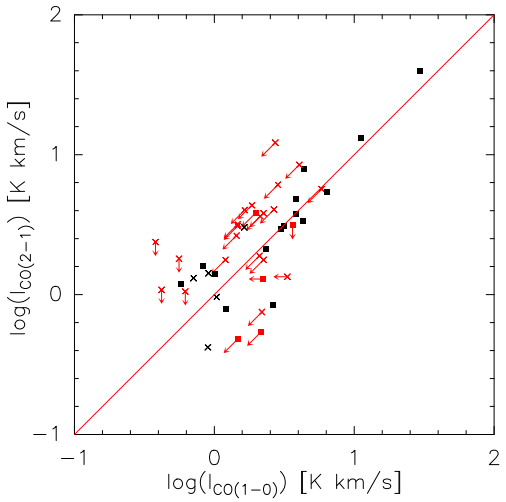

Fig. 13. log($I_{CO(2-1)}$) versus log($I_{CO(1-0)}$) for the galaxies observed by us. Spiral galaxies (T≥1) are shown as filled squares and early-type (T≤0) as crosses. Red symbols indicate upper limits in either $I_{CO(2-1)}$ or $I_{CO(1-0)}$, and black symbols are detections. The y=x line is plotted as reference and does not represent a fit to the data.

5. A possible evolutionary sequence of the molecular gas content and SFR in HCGs

In contrast to the HI content which can be highly deficient, the mean deficiencies for both M_{H_2} and L_{FIR} are low, close to the values found for isolated galaxies. In the case of M_{H_2} we even find indications for an 40-60% excess compared to isolated galaxies. The difference in deficiency between the atomic and molecular gas is most likely due to the larger extent of the HI gas, which can thus be removed more efficiently from the galaxies, while the molecular gas, which is typically more concentrated in the inner regions, is presumably less affected by the environment. Subsequently, the lower HI mass might cause a lower M_{H_2} which leads to a lower SFR. It is, however, remarkable that galaxies with a high HI deficiency can still contain a considerable amount of molecular gas and continue to form stars with a normal SFE. This SF is not expected to last very long because once the molecular gas is used up, no HI is available to provide fuel for future SF.

Within this general picture of relative normality of M_{H_2} and L_{FIR}, we have found a relation between defM_{HI}) and the sSFR, and a tentative trend with defM_{H_2}) and def(L_{FIR}). Furthermore, there is a trend of Def(M_{H_2}) with the evolutionary phase (Tab. 7), in the sense that galaxies in HCGs belonging to phase 1 have the highest excess in M_{H_2}. These trends might suggest that two mechanisms are at play. First, an increasing M_{HI} deficiency can be interpreted within a scenario in which galaxies in HCGs lose part of their HI as a result of mostly tidal stripping during the initial evolutionary phase, as suggested in the evolutionary model of Verdes-Montenegro et al. (2001). On the other hand, in an early evolutionary phase the HI-to-H_2 conversion rate might be enhanced as a result of the continuous interactions between galaxies, leading to the enhancement in M_{H_2} that we observe in evolutionary phase 1. This enhancement of M_{H_2} can not explain the high HI deficiencies observed in most galaxies, in agreement with the conclusions of Rasmussen et al. (2008), but it could partly explain the lack of HI, especially in the galaxies with the lowest HI deficiencies.

Based on our results, we thus suggest the following scenario which is speculative but compatible with our observations. Galaxies in a HCG start with a normal content in M_{H_2} and M_{HI}, i.e. they have Def(M_{HI}) = 0 and Def(M_{H_2}) = 0. Then, during the early evolutionary phase tidal interactions enhance the conversion from atomic to molecular gas at the same time as they strip the HI from the galaxies, which leads to Def(M_{HI}) > 0 and Def(M_{H_2}) < 0. Finally, the multiple interactions within the group strip the main part of the HI in the disks, resulting in Def(M_{HI}) >> 0 and, as a consequence also increase in Def(M_{H_2}). This last effect could have contributed to an increase of the fraction of lenticular galaxies along the evolutionary sequence due to HI and H_2 stripping of spirals.

6. Summary and Conclusions

We analyzed data for M_{H_2}, obtained from observations with the IRAM 30m telescope and from the literature, L_{FIR} from IRAS and M_{HI} for 86 galaxies in 20 HCGs in order to study the relation between atomic gas, molecular gas and SFR, traced by L_{FIR}, in these galaxies. We compared these properties to those of isolated galaxies from the AMIGA project (Verdes-Montenegro et al. 2005). We adopted the same CO-to-H_2 conversion factor for both samples. The main conclusions of our study can be summarized as follows:

- The relation between M_{H_2}, L_{FIR} and L_B in galaxies in HCGs is not significantly different from the one found in isolated galaxies. The values of L_{FIR} for spirals galaxies in HCGs are similar to those of the AMIGA galaxies for the same L_B. For M_{H_2} we find, however, a slight, but statistically significant, excess (∼ 50%) of HCGs spiral galaxies relative to AMIGA galaxies. This could alternatively be explained by a higher radial concentration of the molecular gas in HCG galaxies to the center when compared with isolated galaxies, so that the extrapolation of the flux based on a similar extent (see Sec. 3.1.3) would lead to an overestimate of M_{H_2} for the group galaxies. Another possible explanation for this difference could be a systematically lower CO-to-H_2 conversion factor for spirals in HCGs.
- For elliptical and S0 galaxies the large number of upper limits do not allow strong conclusions about their M_{H_2} or L_{FIR}. We note however that, while for S0s the L_B range is comparable to isolated S0 galaxies, Es in HCGs are up to half an order magnitude more luminous in L_B than isolated Es.
- Practically all of our galaxies lie in the range of L_{FIR}/M_{H_2}=1-10 $L_\odot/M_\odot$, typical for normal, quiescent galaxies. The deficiencies in M_{H_2} and L_{FIR} are tightly correlated and span about the same range as in isolated galaxies.
- The M_{HI} deficiency, calculated from the VLA data for individual galaxies, is much larger than the other deficiencies with a mean value of 0.93±0.13 (12% of the expected value) for spiral galaxies, and 1.31±0.11 (5% the expected value) for all morphological types, and represents the largest difference with respect to isolated galaxies. Those values are significantly larger than those obtained in Verdes-Montenegro et al. (2001) since the sample in that

study was biased towards HI bright galaxies while here we present a redshift selected sample.
- The SFE of the spiral galaxies in the HCGs is slightly lower than in isolated galaxies, but in the range of values found for nearby spiral galaxies (Bigiel et al. 2011). We have found no relation of the SFE with neither Def($M_{\rm HI}$) nor Def($M_{\rm H_2}$).
- There is a trend of the sSFR to increase with decreasing Def($M_{\rm HI}$) and Def($M_{\rm H_2}$). This suggests that, although the Def($M_{\rm HI}$) of a galaxy has only a weak influence on the absolute SFR, it has a stronger influence on the SFR per stellar mass.
- There is a trend of decreasing molecular gas deficiency with evolutionary phase, with galaxies in groups in an early phase showing an excess in $M_{\rm H_2}$. This excess goes to 0 in later phases. A similar trend might exist with def($M_{\rm HI}$), but is statistically only marginally significant in our sample. This is interpreted as an initial enhancement of the conversion from atomic to molecular gas due to on-going tidal interactions, later followed by stripping of most of their HI. In these later phases, evolution of spiral to lenticular galaxies, would both explain the overabundance of those morphological types as well as the $M_{\rm HI}$ deficiency and decrease in $M_{\rm H_2}$ content of the galaxies.
- No trend with the global HI deficiency of the groups is found, which suggest that the molecular gas content and SF are more driven by one-to-one interaction than directly by the local environment.

Acknowledgements. This work has been supported by the research projects AYA2008-06181-C02 and AYA2007-67625-C02-02 from the Spanish Ministerio de Ciencia y Educación and the Junta de Andalucía (Spain) grants P08-FQM-4205, FQM-0108 and TIC-114. DE was supported by a Marie Curie International Fellowship within the 6th European Community Framework Programme (MOIF-CT-2006-40298). UL warmly thanks IPAC (Caltech), where this work was finished during a sabbatical stay, for their hospitality. We also thank T. Bitsakis and V. Charmandaris for letting us use their Spitzer data prior to publication, and the anonymous referee for critical comments helping to put our conclusions on a firmer ground and improving the quality of the paper. This work is based on observations with the Instituto de Radioastronomia Milimétrica IRAM 30m and the Five College Radio Astronomy (FCRAO) 14m. The FCRAO is supported by NSF grant AST 0838222. This research has made use of the NASA/IPAC Extragalactic Database (NED) which is operated by the Jet Propulsion Laboratory, California Institute of Technology, under contract with the National Aeronautics and Space Administration. We also acknowledge the usage of the HyperLeda database (http://leda.univ-lyon1.fr).

References

Bekki, K. & Couch, W. J. 2011, MNRAS, 415, 1783
Bell, E. F. 2003, ApJ, 586, 794
Bell, E. F., McIntosh, D. H., Katz, N., & Weinberg, M. D. 2003, ApJS, 149, 289
Bigiel, F., Leroy, A. K., Walter, F., et al. 2011, ApJ, 730, L13+
Bitsakis, T., Charmandaris, V., da Cunha, E., et al. 2011, A&A, 533, A142+
Bitsakis, T., Charmandaris, V., Le Floc'h, E., et al. 2010, A&A, 517, A75+
Borthakur, S., Yun, M. S., & Verdes-Montenegro, L. 2010, ApJ, 710, 385
Boselli, A., Gavazzi, G., Lequeux, J., et al. 1997, A&A, 327, 522
Boselli, A., Lequeux, J., & Gavazzi, G. 2002, A&A, 384, 33
Boselli, A., Mendes de Oliveira, C., Balkowski, C., Cayatte, V., & Casoli, F. 1996, A&A, 314, 738
Braine, J., Combes, F., Casoli, F., et al. 1993, A&AS, 97, 887
Calzetti, D., Wu, S., Hong, S., et al. 2010, ApJ, 714, 1256
Casasola, V., Bettoni, D., & Galletta, G. 2004, A&A, 422, 941
Casoli, F., Boisse, P., Combes, F., & Dupraz, C. 1991, A&A, 249, 359
Cole, S., Norberg, P., Baugh, C. M., et al. 2001, MNRAS, 326, 255
de Vaucouleurs, G., de Vaucouleurs, A., Corwin, Jr., H. G., et al. 1991, Third Reference Catalogue of Bright Galaxies, ed. de Vaucouleurs, G., de Vaucouleurs, A., Corwin, H. G., Jr., Buta, R. J., Paturel, G., & Fouque, P.
Dickman, R. L., Snell, R. L., & Schloerb, F. P. 1986, ApJ, 309, 326
Durbala, A., del Olmo, A., Yun, M. S., et al. 2008, AJ, 135, 130
Feigelson, E. D. & Nelson, P. I. 1985, ApJ, 293, 192
Fernández-Lorenzo, M. 2011, A&A, submitted
Fumagalli, M., Krumholz, M. R., Prochaska, J. X., Gavazzi, G., & Boselli, A. 2009, ApJ, 697, 1811
Haynes, M. P. & Giovanelli, R. 1984, AJ, 89, 758
Helou, G., Khan, I. R., Malek, L., & Boehmer, L. 1988, ApJS, 68, 151
Hickson, P. 1982, ApJ, 255, 382
Hickson, P., Mendes de Oliveira, C., Huchra, J. P., & Palumbo, G. G. 1992, ApJ, 399, 353
Hickson, P., Menon, T. K., Palumbo, G. G. C., & Persic, M. 1989, ApJ, 341, 679
Iglesias-Páramo, J. & Vílchez, J. M. 1999, ApJ, 518, 94
Jarrett, T. H., Chester, T., Cutri, R., et al. 2000, AJ, 119, 2498
Karachentseva, V. E. 1973, Soobshcheniya Spetsial'noj Astrofizicheskoj Observatorii, 8, 3
Kenney, J. D. & Young, J. S. 1986, ApJ, 301, L13
Kennicutt, Jr., R. C. 1998, ARA&A, 36, 189
Kroupa, P. 2001, MNRAS, 322, 231
Lavalley, M. P., Isobe, T., & Feigelson, E. D. 1992, in Bulletin of the American Astronomical Society, Vol. 24, Bulletin of the American Astronomical Society, 839–840
Leon, S., Combes, F., & Menon, T. K. 1998, A&A, 330, 37
Leon, S., Verdes-Montenegro, L., Sabater, J., et al. 2008, A&A, 485, 475
Leroy, A. K., Walter, F., Bigiel, F., et al. 2009, AJ, 137, 4670
Leroy, A. K., Walter, F., Brinks, E., et al. 2008, AJ, 136, 2782
Lisenfeld, U., Espada, D., Verdes-Montenegro, L., et al. 2011, A&A, 534, A102+
Lisenfeld, U., Verdes-Montenegro, L., Sulentic, J., et al. 2007, A&A, 462, 507
Maloney, P. & Black, J. H. 1988, ApJ, 325, 389
Menon, T. K. 1995, MNRAS, 274, 845
Narayanan, D., Krumholz, M., Ostriker, E. C., & Hernquist, L. 2011, MNRAS, 418, 664
Nishiyama, K., Nakai, N., & Kuno, N. 2001, PASJ, 53, 757
Rasmussen, J., Ponman, T. J., Verdes-Montenegro, L., Yun, M. S., & Borthakur, S. 2008, MNRAS, 388, 1245
Regan, M. W., Thornley, M. D., Helfer, T. T., et al. 2001, ApJ, 561, 218
Rubin, V. C., Hunter, D. A., & Ford, Jr., W. K. 1990, ApJ, 365, 86
Sulentic, J. W. & de Mello Rabaca, D. F. 1993, ApJ, 410, 520
Verdes-Montenegro, L., Sulentic, J., Lisenfeld, U., et al. 2005, A&A, 436, 443
Verdes-Montenegro, L., Yun, M. S., Borthakur, S., et al. 2007, in Groups of Galaxies in the Nearby Universe, ed. I. Saviane, V. D. Ivanov, & J. Borissova, 349–+
Verdes-Montenegro, L., Yun, M. S., Perea, J., del Olmo, A., & Ho, P. T. P. 1998, ApJ, 497, 89
Verdes-Montenegro, L., Yun, M. S., Williams, B. A., et al. 2001, A&A, 377, 812
Xu, C. & Sulentic, J. W. 1991, ApJ, 374, 407
Young, J. S. & Scoville, N. Z. 1991, ARA&A, 29, 581

Appendix A: CO spectra

Figure A.1 shows the CO(1-0) spectra of the detections and tentative detections observed by us and Figure A.1 the CO(2-1) spectra.

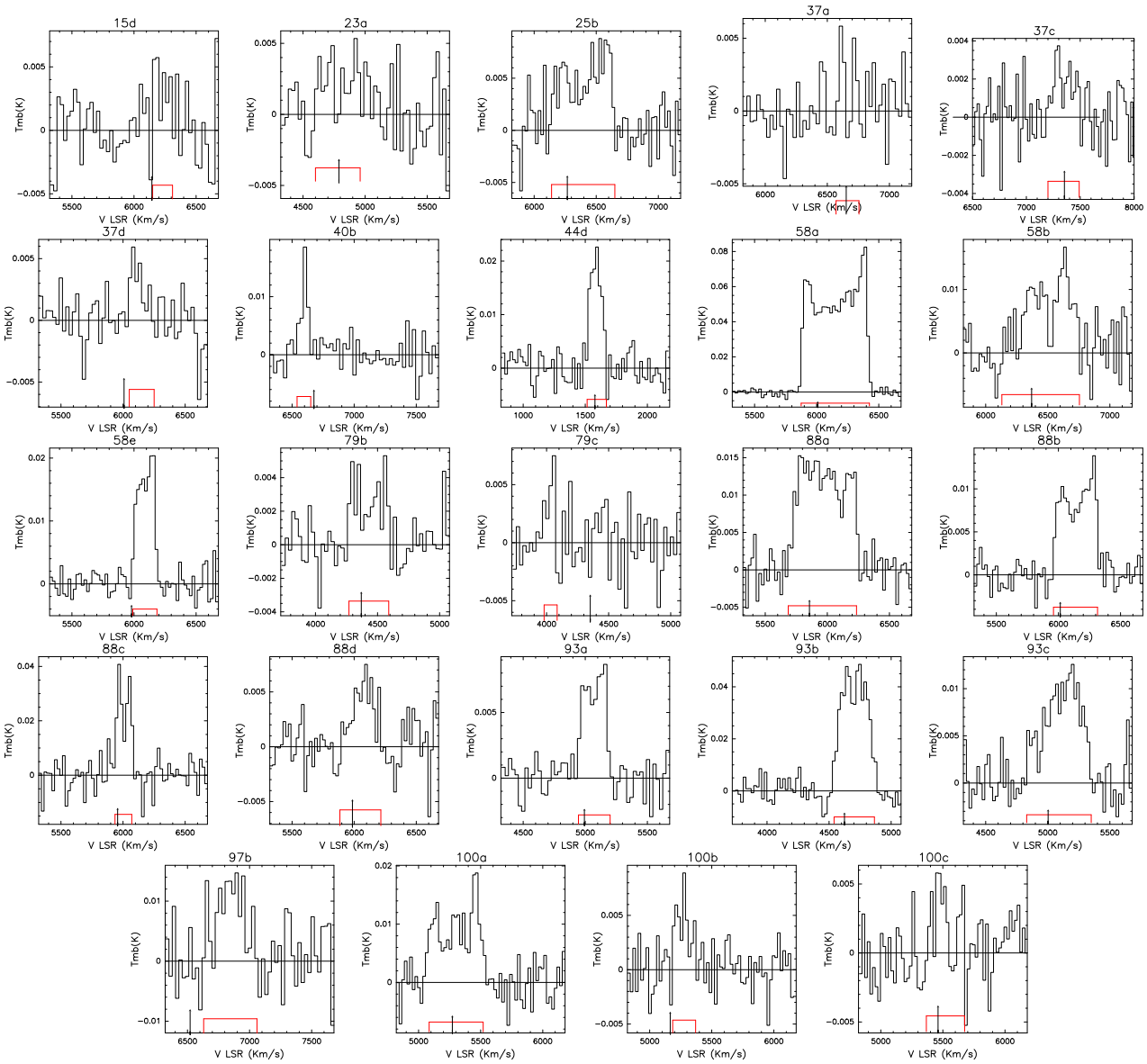

Fig. A.1. CO(1-0) spectra for the detected HCG galaxies. The detection window is shown with a red horizontal line. Main beam temperature ($T_{\rm mb}$, in K) is displayed in the Y axis, and the velocity with respect to LSR in km s^{-1} is displayed in X axis. Velocity resolution is smoothed to 21 or 27 km s^{-1}. The optical velocity of the galaxy, converted to the radio definition, is marked with an arrow.

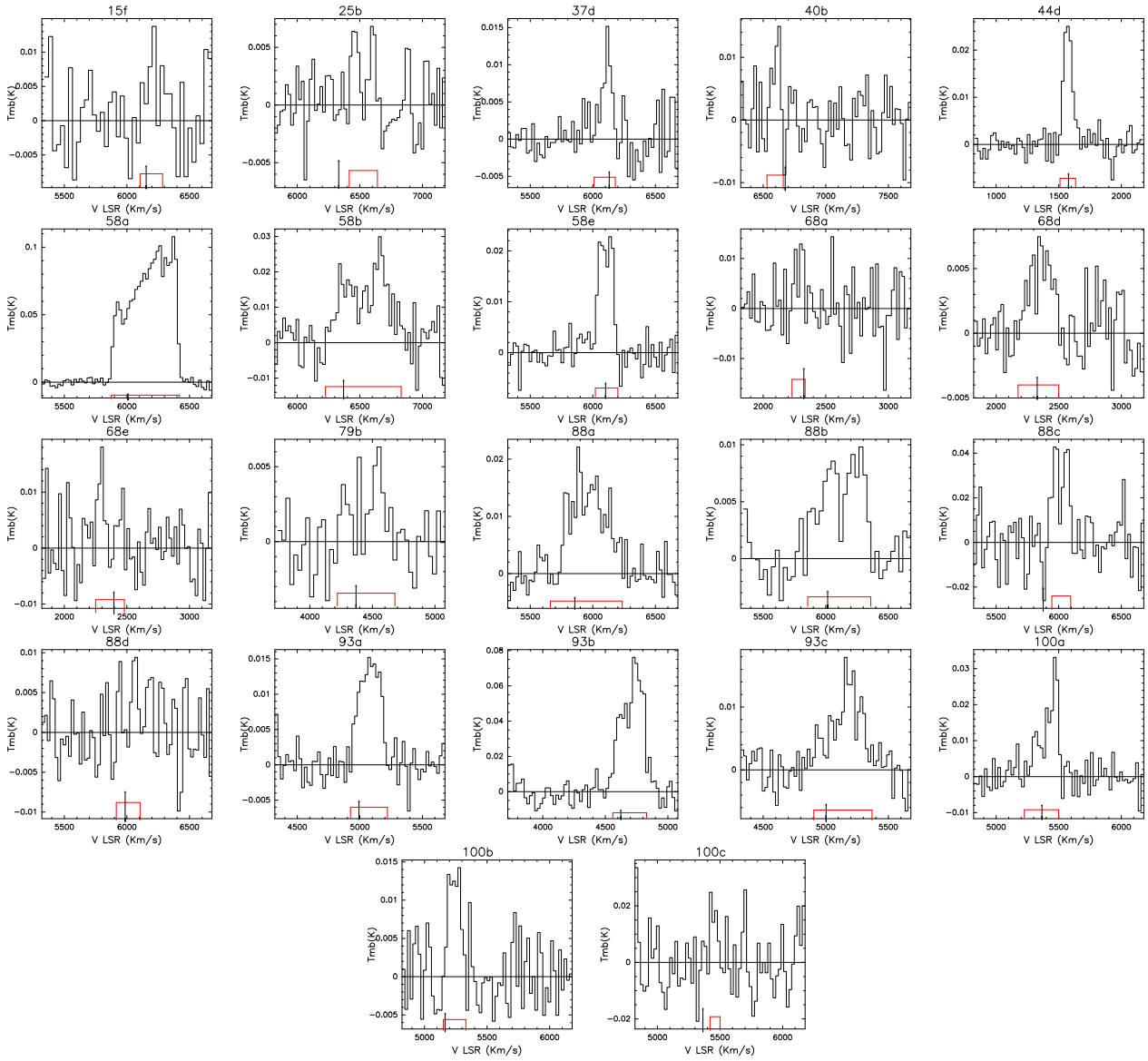

Fig. A.2. CO(2-1) spectra for the detected HCG galaxies. The detection window is shown with a red horizontal line. Main beam temperature ($T_{\rm mb}$, in K) is displayed in the Y axis, and the velocity with respect to LSR in km s^{-1} is displayed in X axis. Velocity resolution is smoothed to 21 or 27 km s^{-1}. The optical velocity of the galaxy, converted to the radio definition, is marked with an arrow.

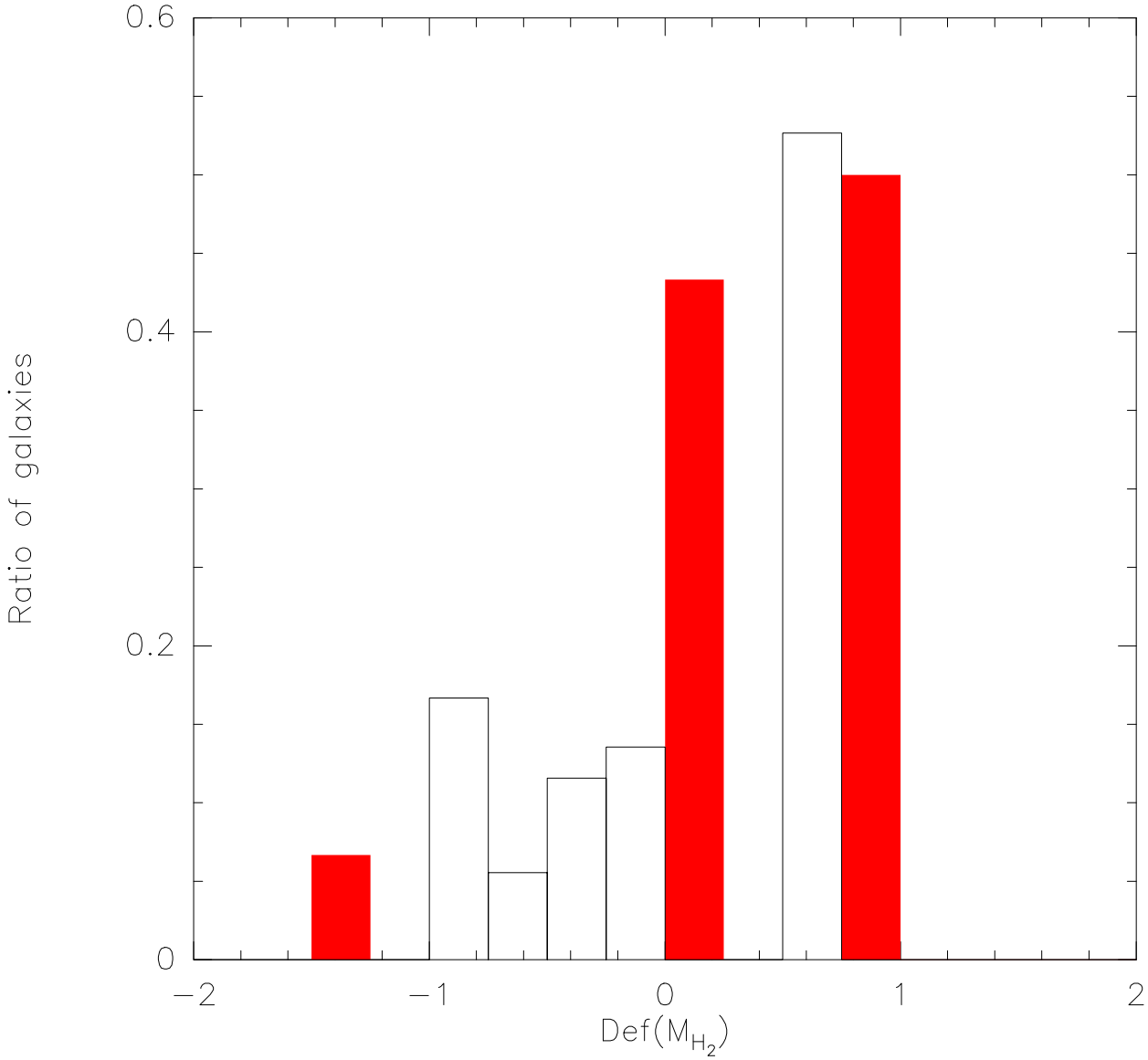
0.6
0.4
0.2
0
Ratio of galaxies
−2
−1
0
1
2
Def(M$_{H_2}$)

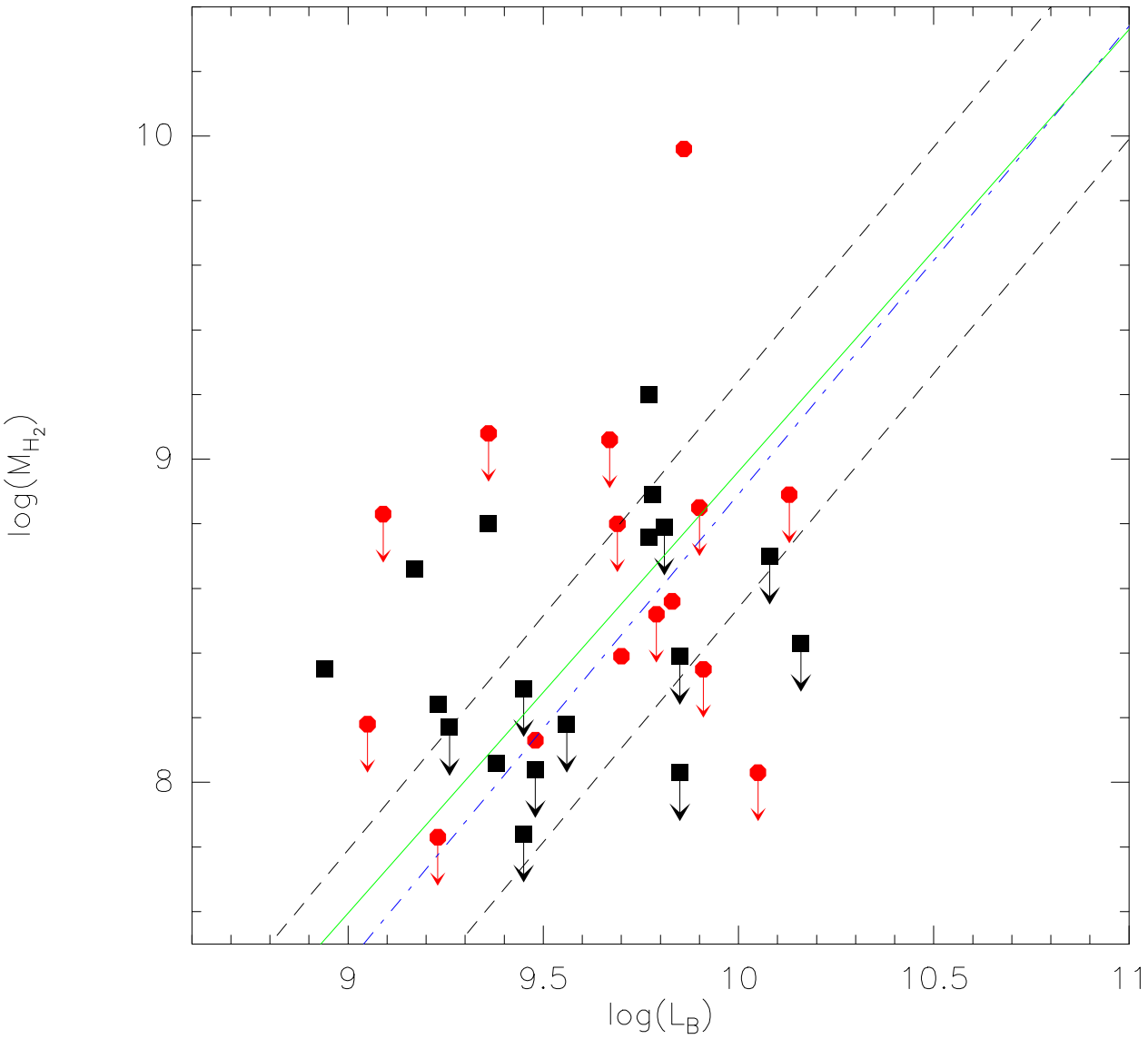
10
9
8
log(M_H2)
9
9.5
10
10.5
11
log(L_B)

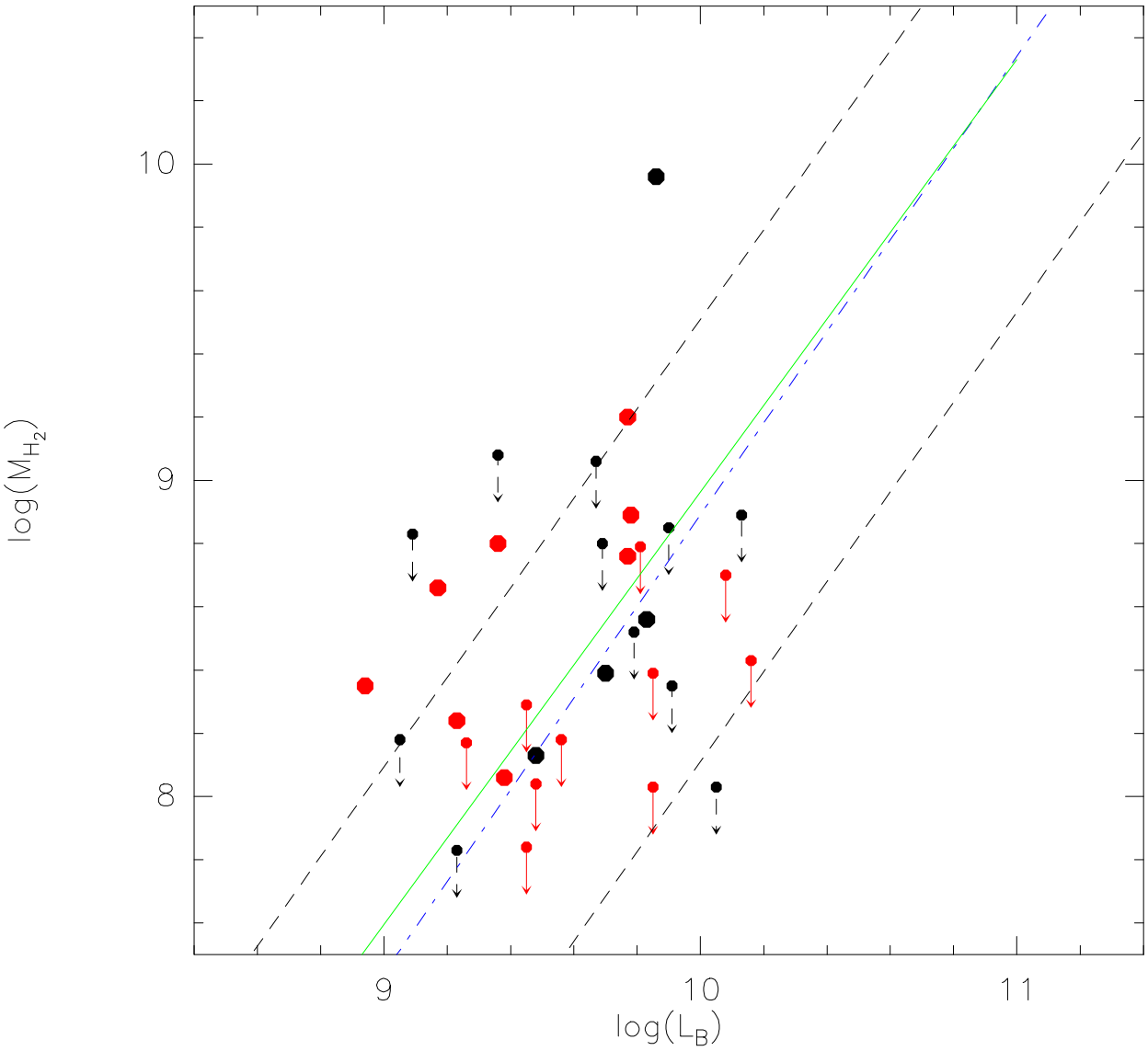
10
9
8
log(M_H2)
9
10
11
log(L_B)

0.2
0.1
0
Ratio of galaxies Phase 1

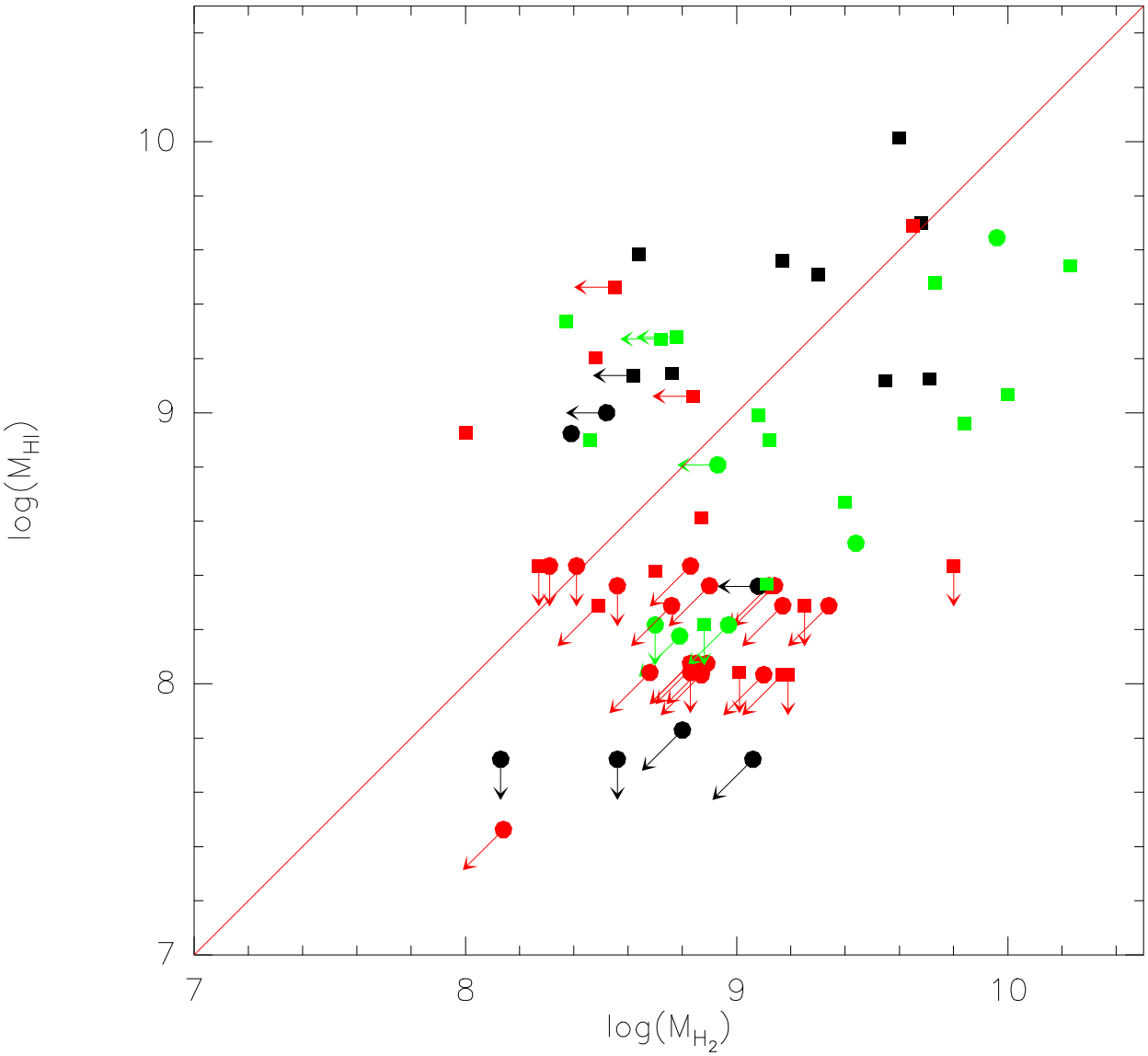
10
9
8
7
7
8
9
10
log(M_HI)
log(M_H2)

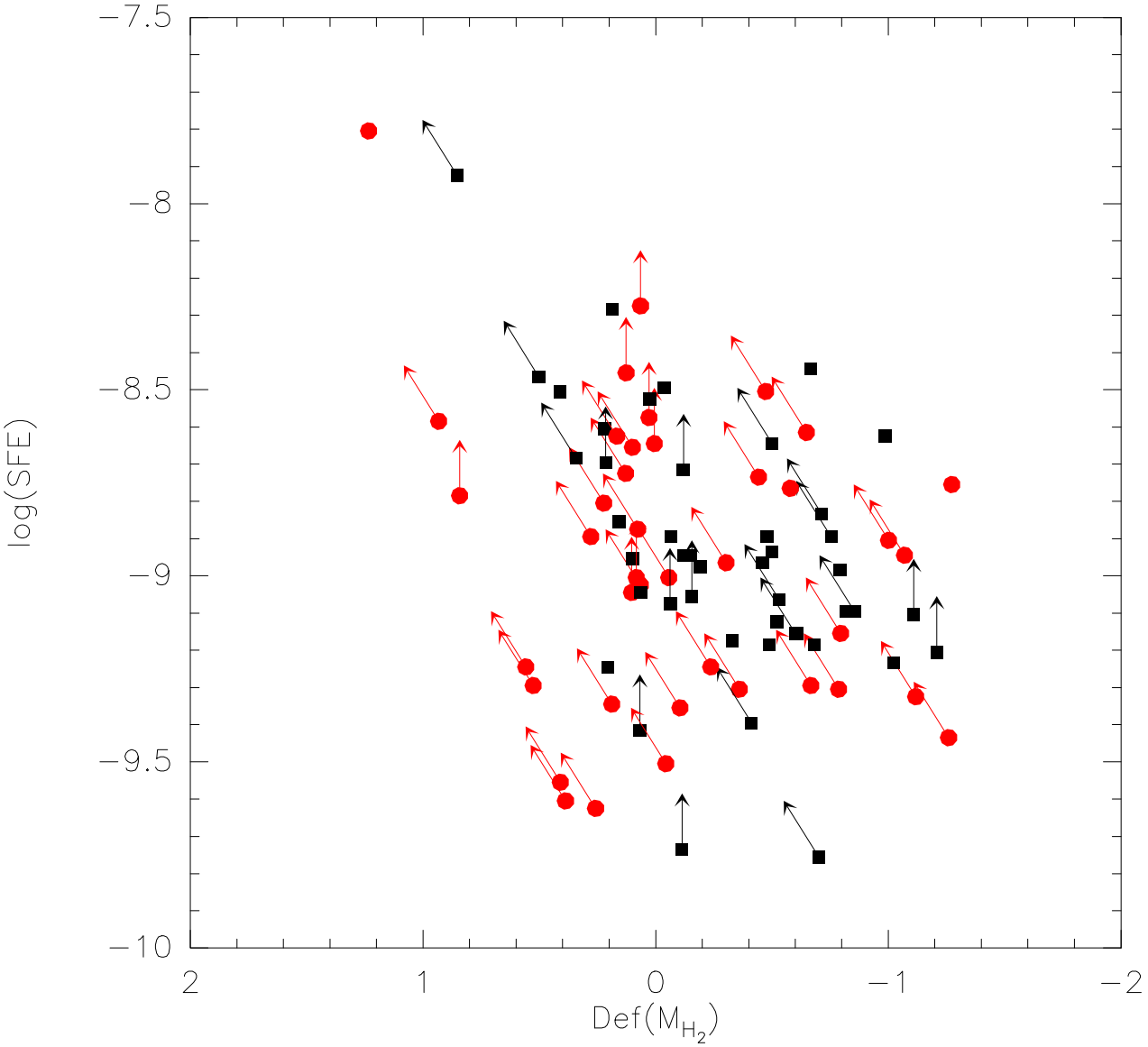
−7.5
−8
−8.5
−9
−9.5
−10
log(SFE)
2
1
0
−1
−2
Def(M$_{H_2}$)

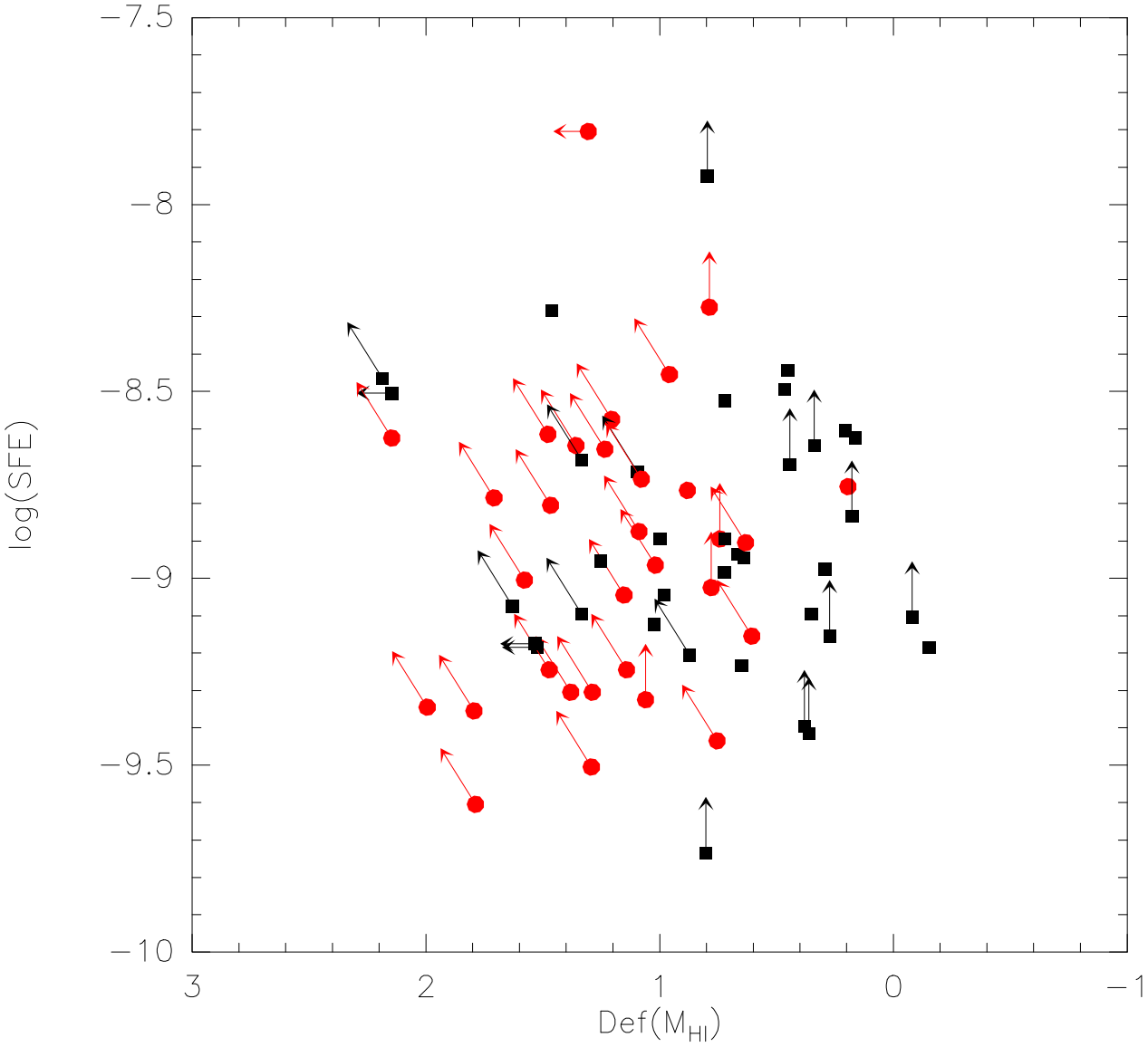
−7.5
−8
−8.5
−9
−9.5
−10
log(SFE)
3
2
1
0
−1
Def(M_HI)

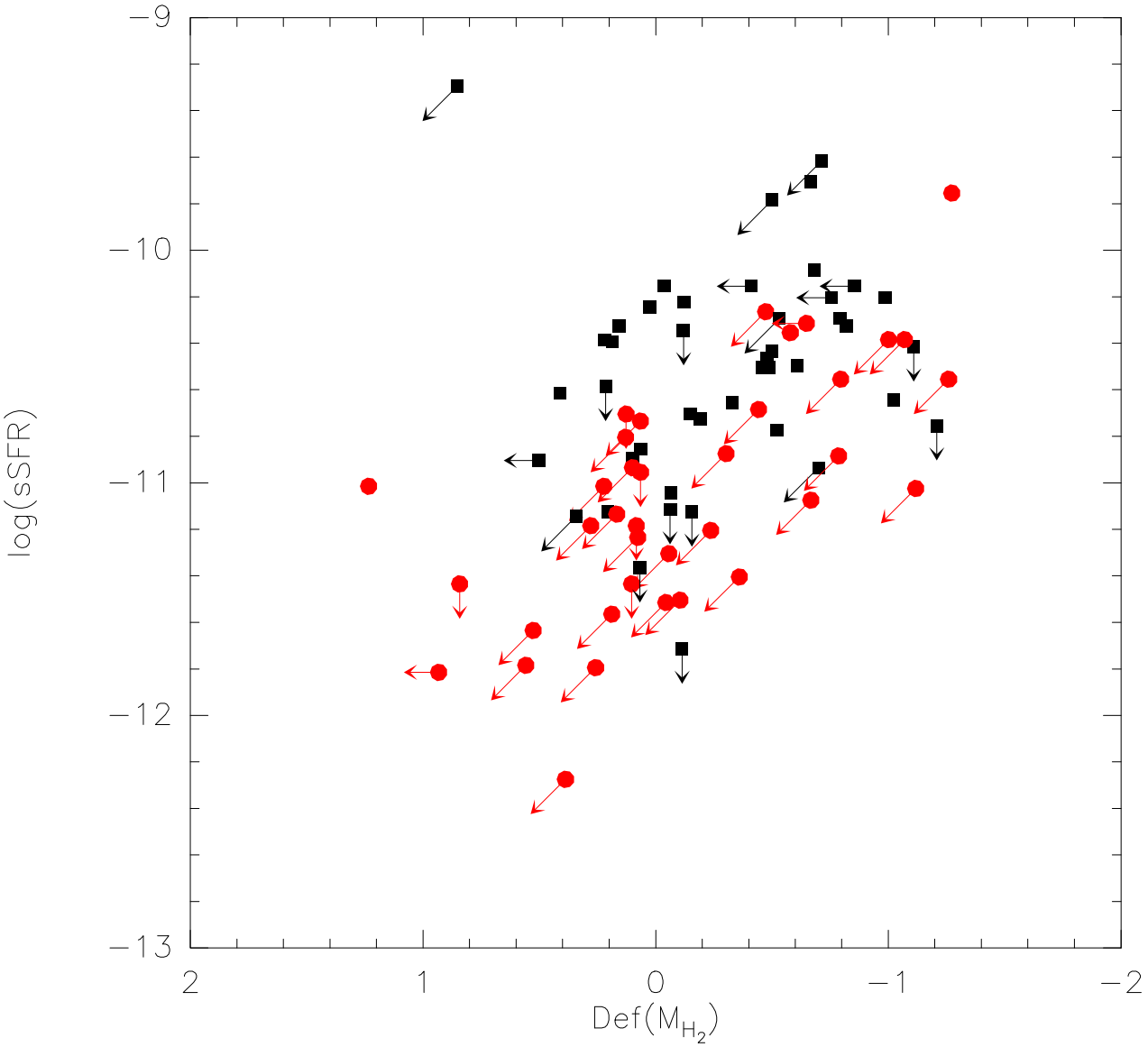
−9
−10
−11
−12
−13
log(sSFR)
2
1
0
−1
−2
Def(M$_{H_2}$)

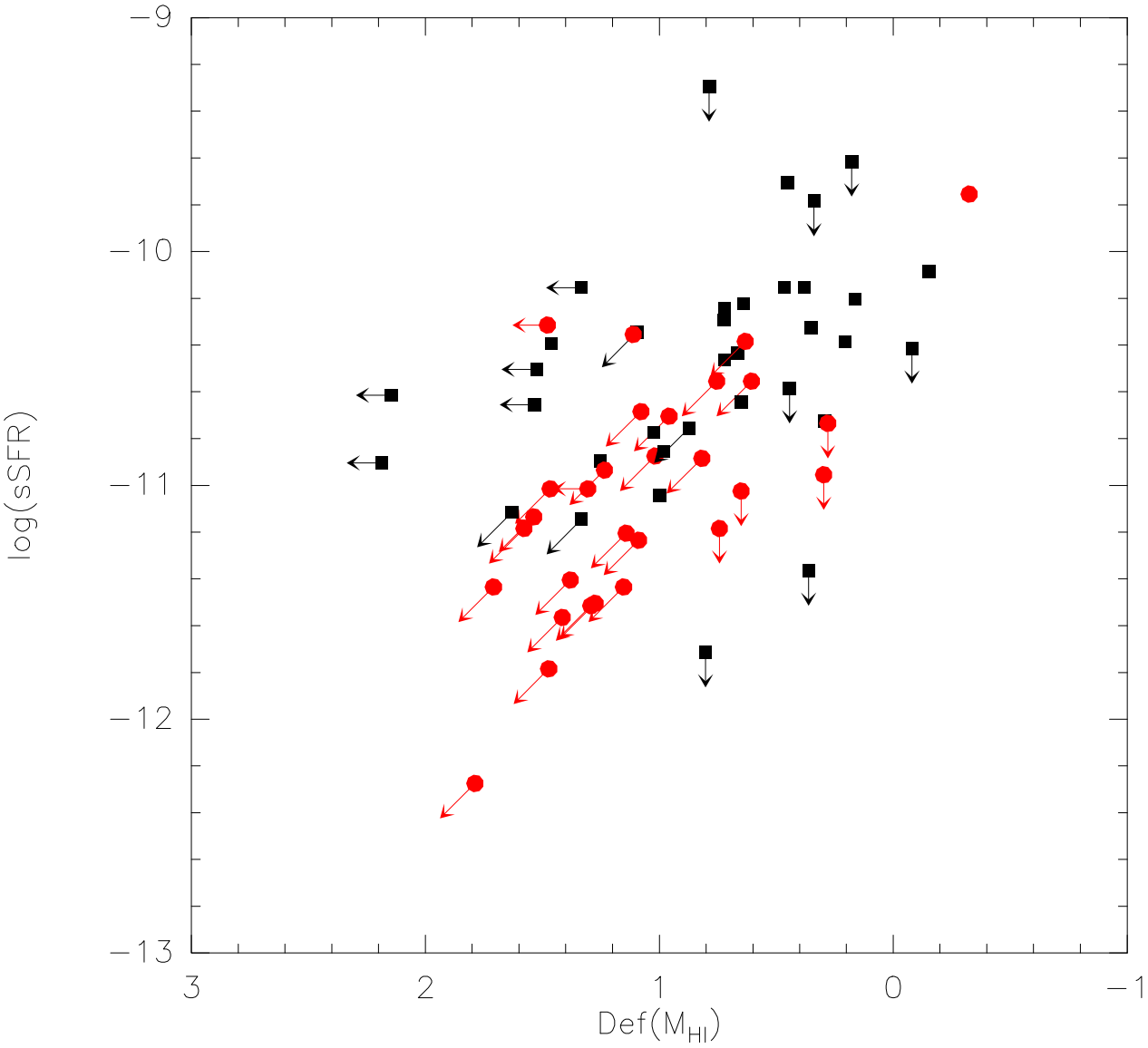
−9
−10
−11
−12
−13
log(sSFR)
3
2
1
0
−1
Def(M_HI)

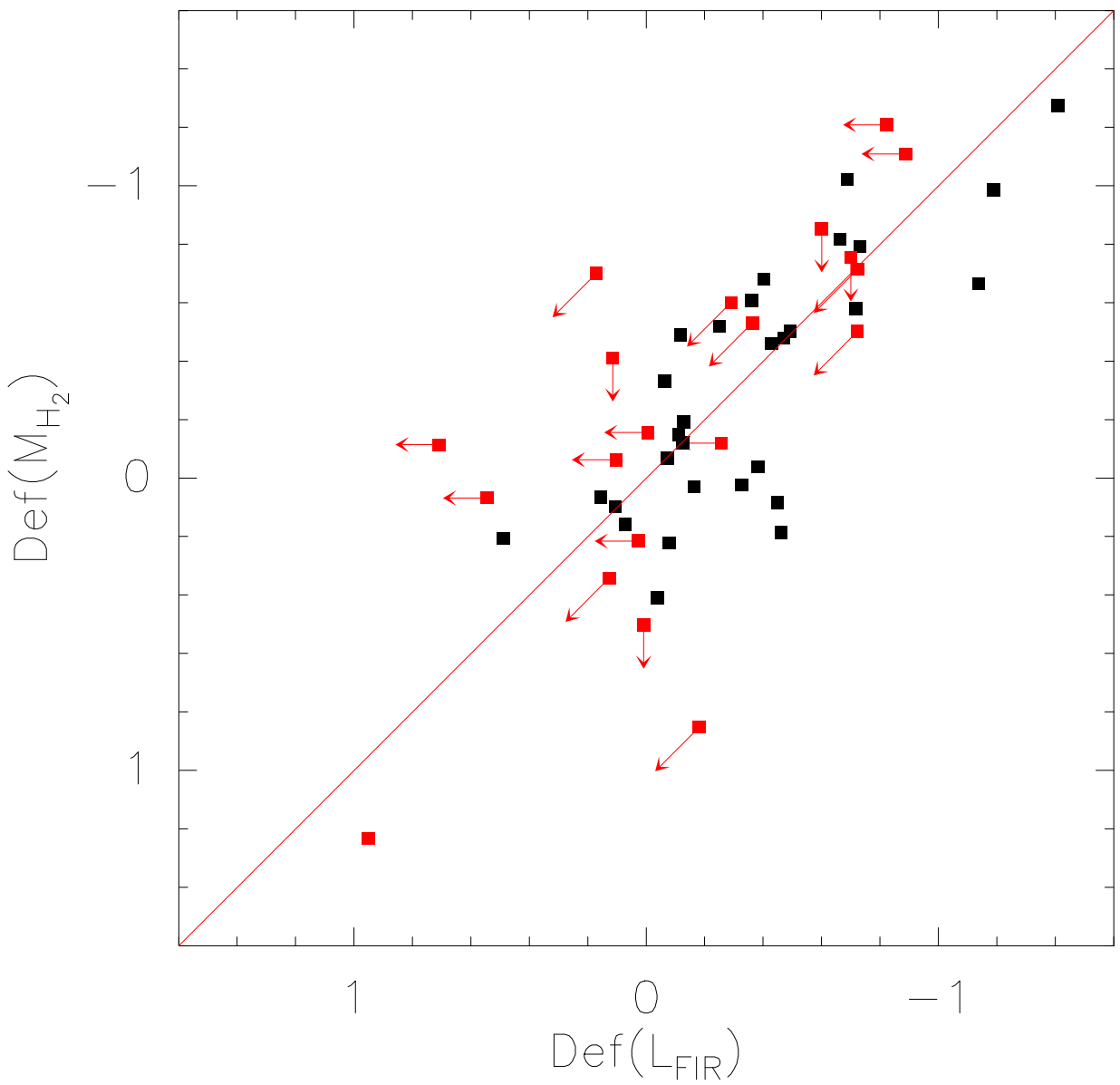
Def(M_{H_2})
−1
0
1
1
0
−1
Def(L_{FIR})

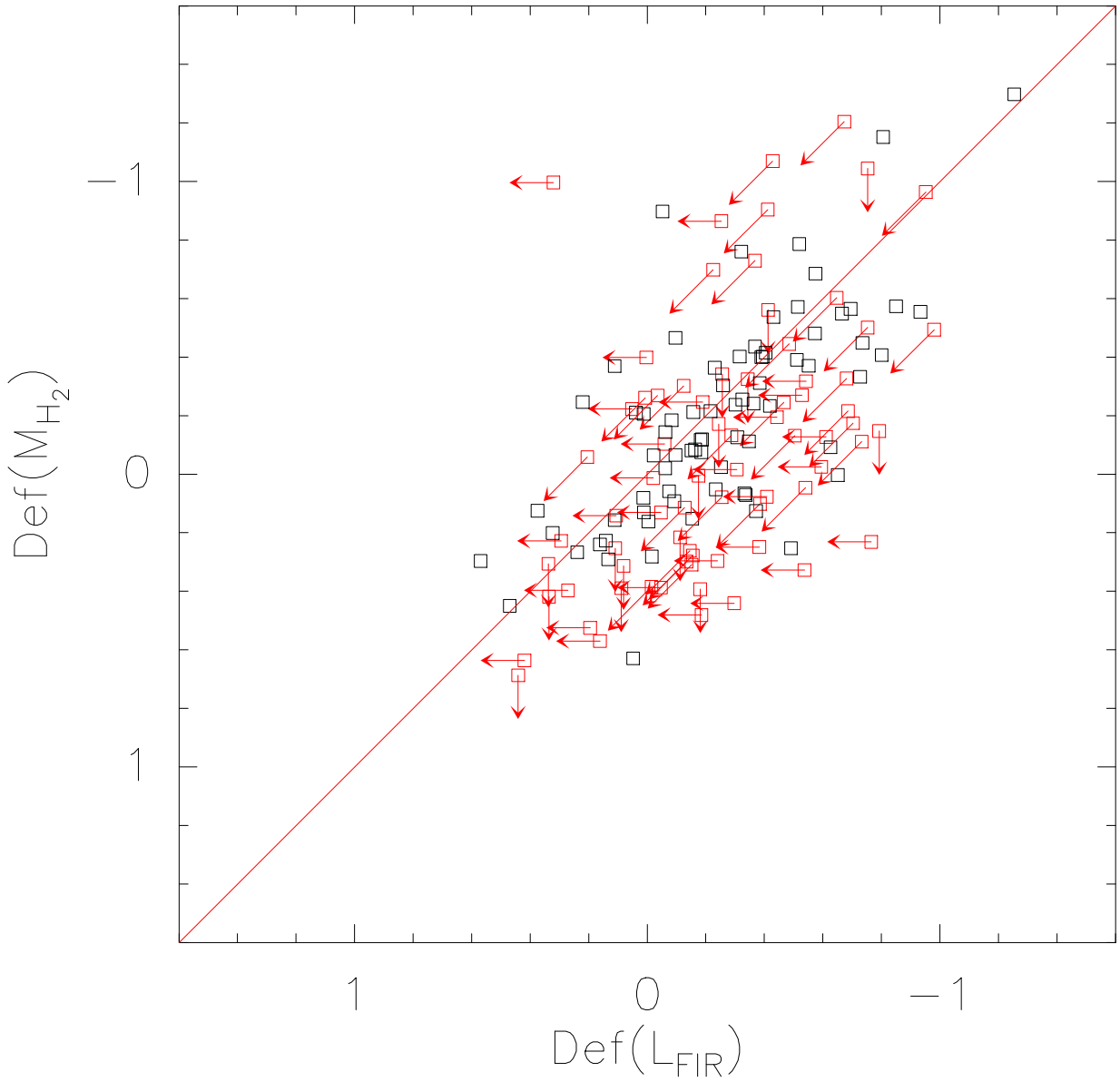
−1
0
1
Def(M_H2)
1
0
−1
Def(L_FIR)

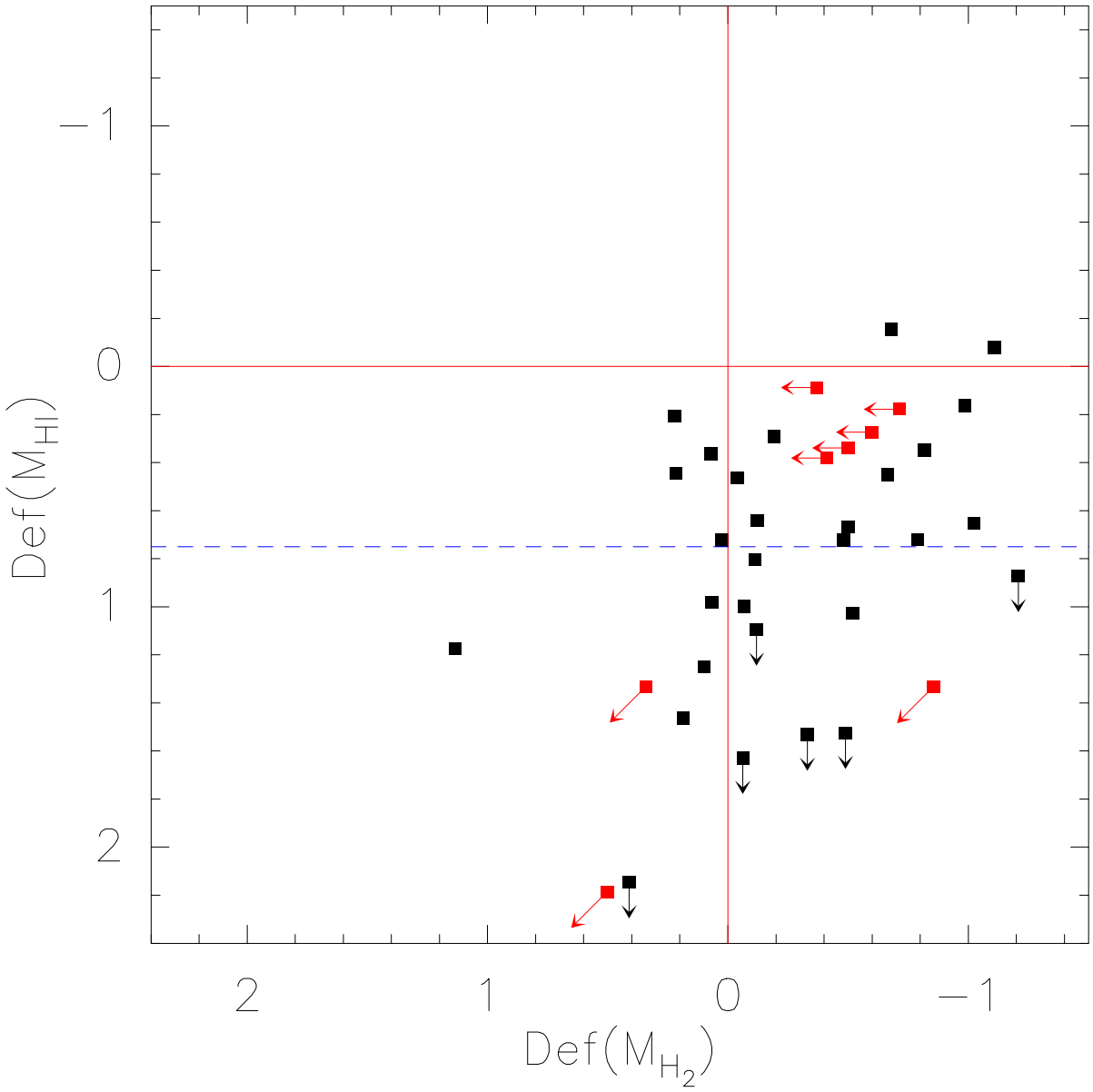
−1
0
1
2
Def(M_HI)
2
1
0
−1
Def(M_H2)

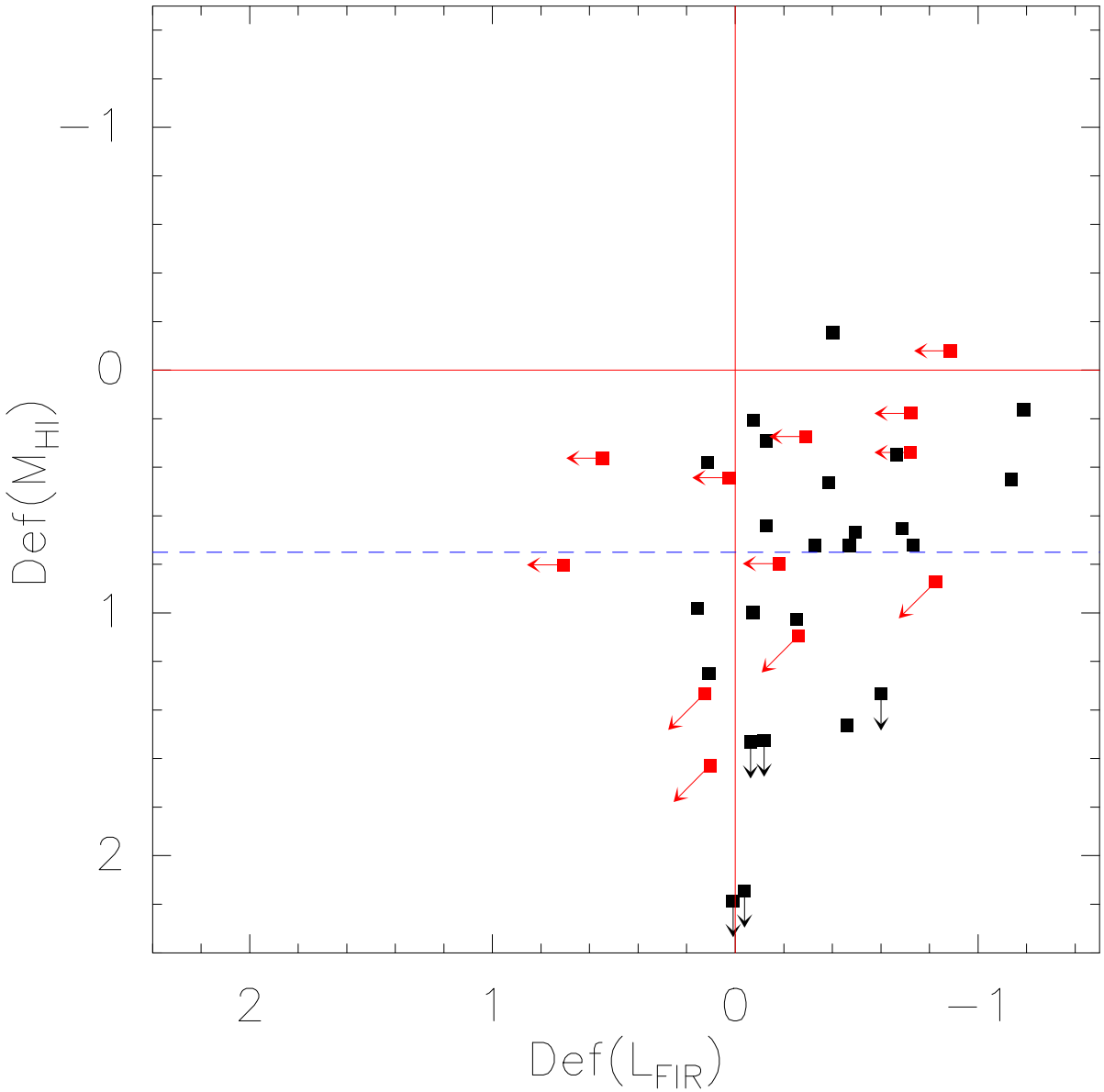
−1
0
1
2
Def(M_HI)
2
1
0
−1
Def(L_FIR)

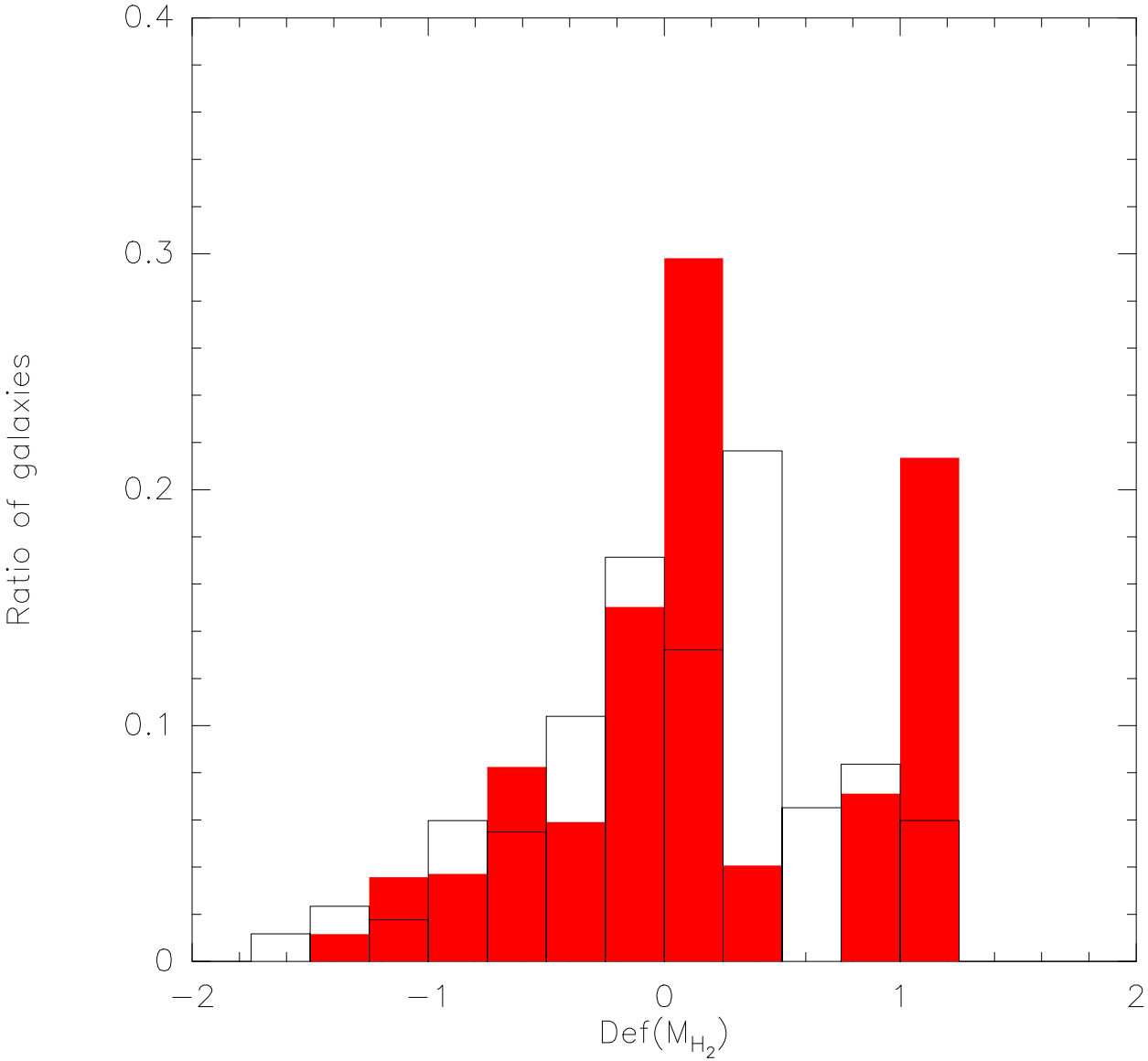
0.4
0.3
0.2
0.1
0
Ratio of galaxies
−2
−1
0
1
2
Def(M$_{H_2}$)

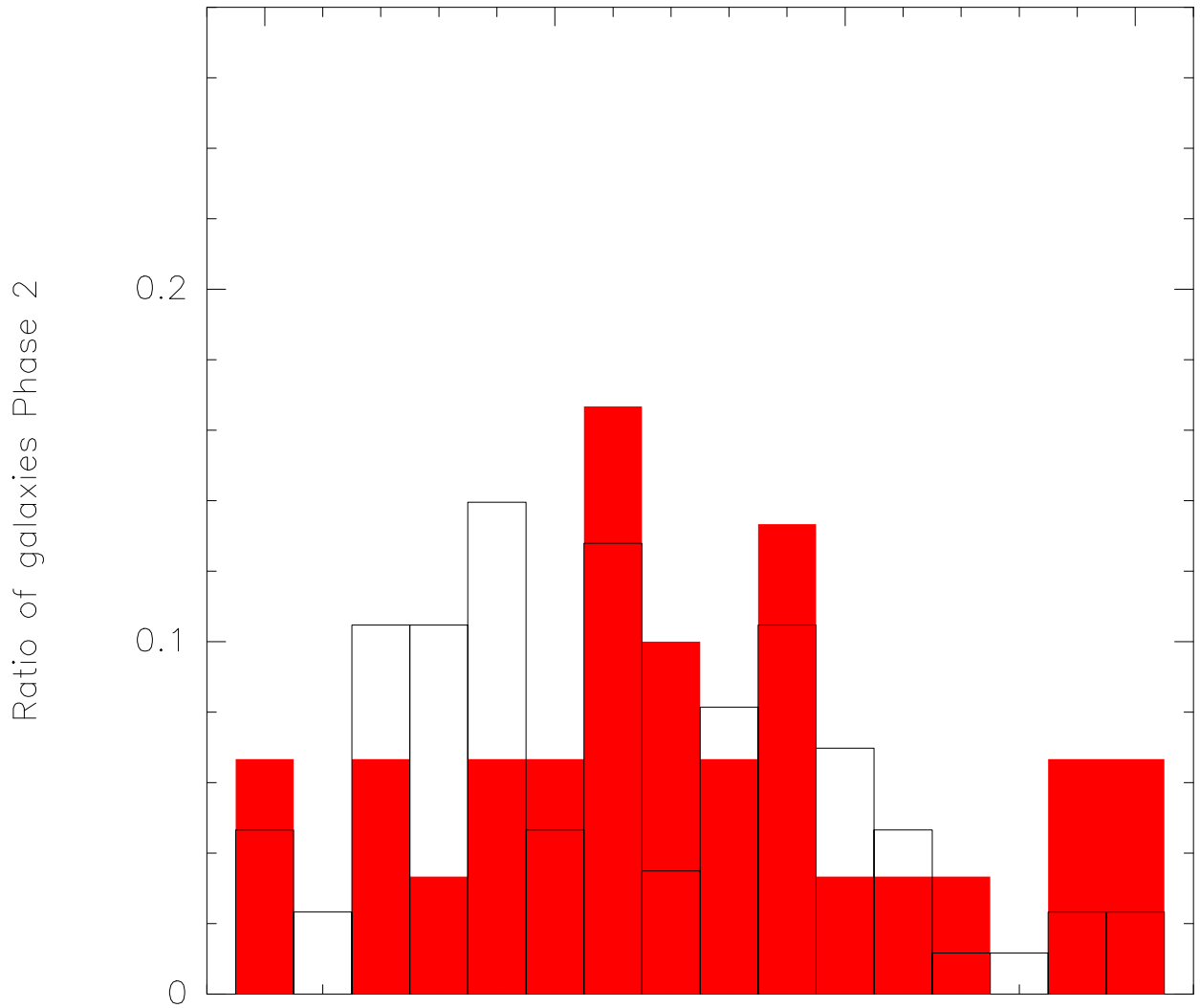
Ratio of galaxies Phase 2
0.2
0.1
0

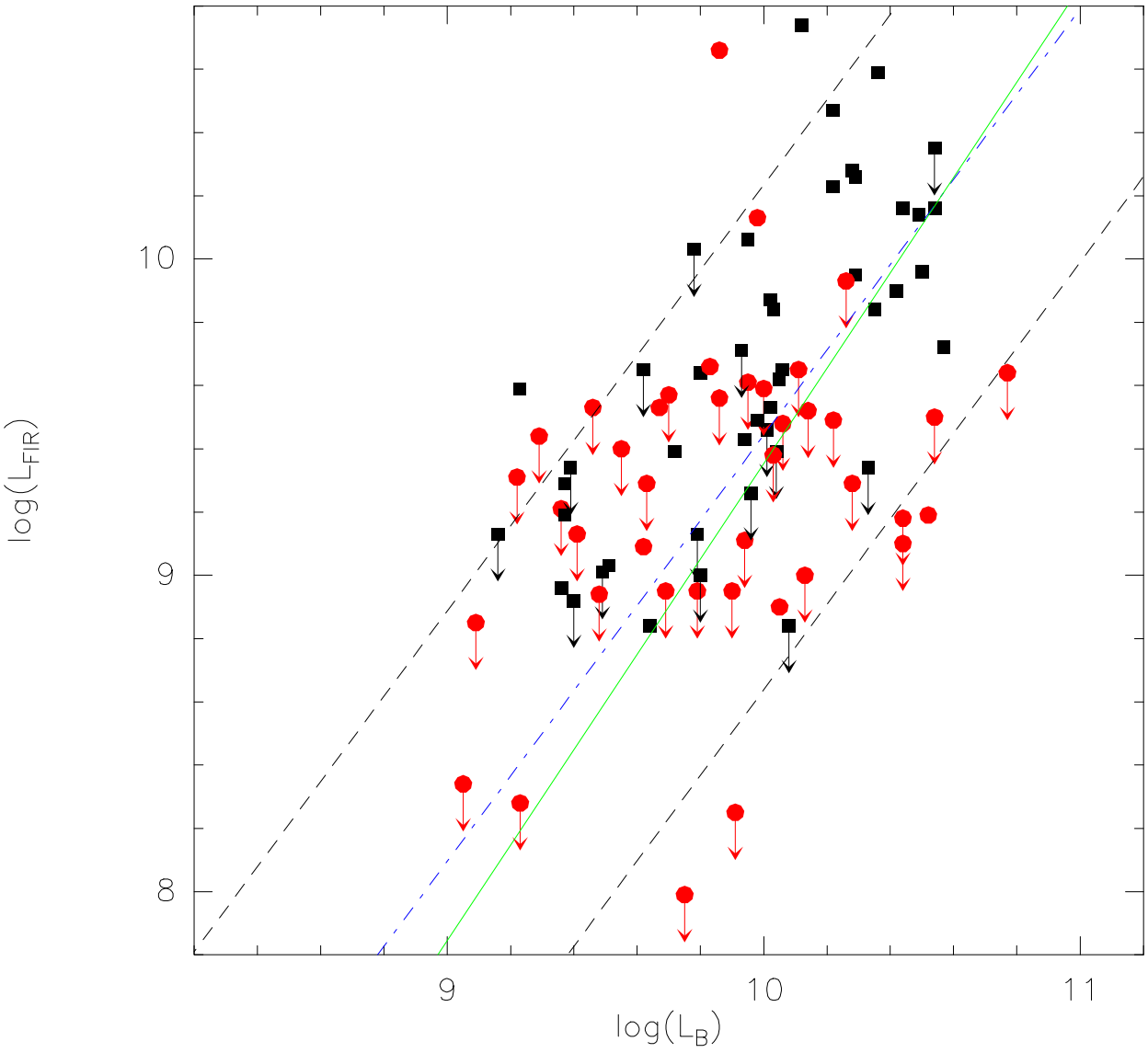
10
9
8
log(L_FIR)
9
10
11
log(L_B)

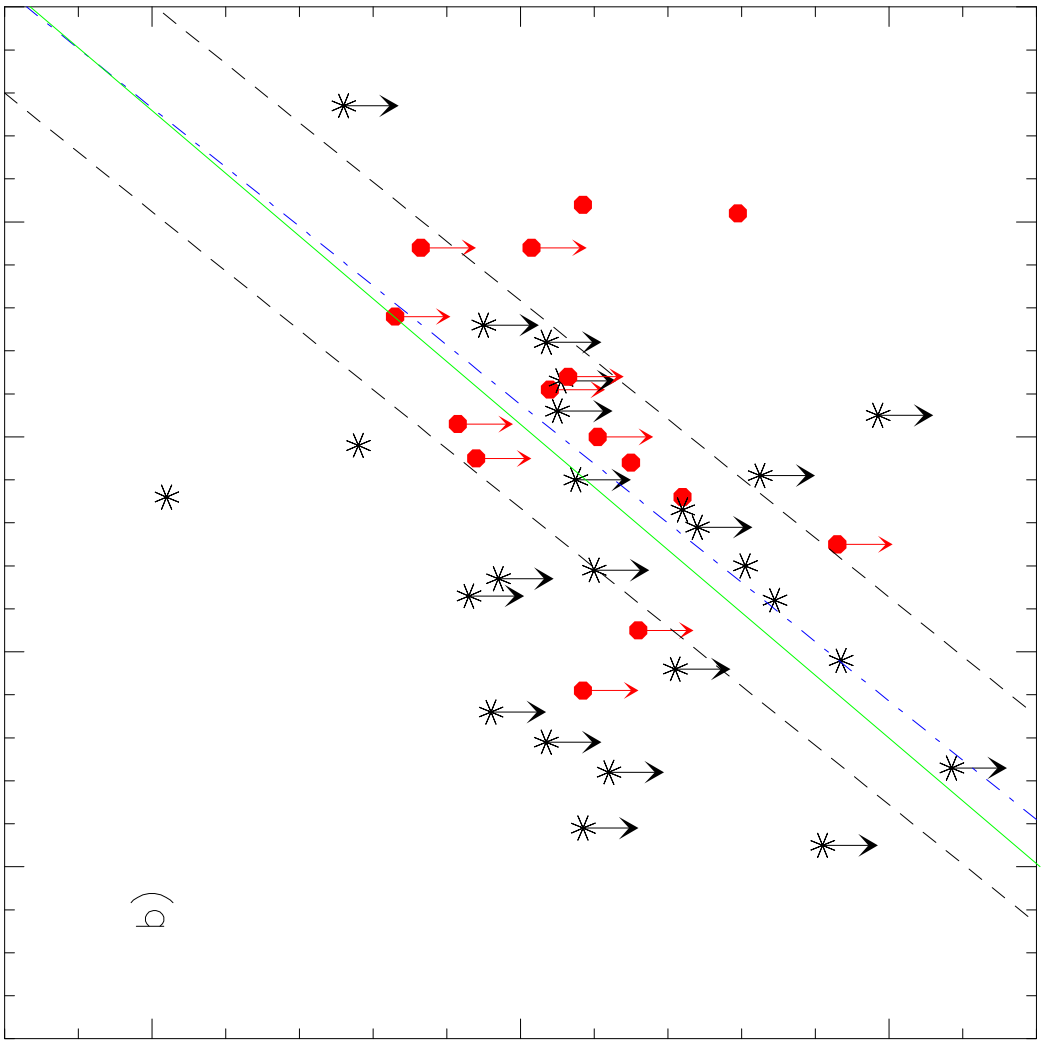
b)

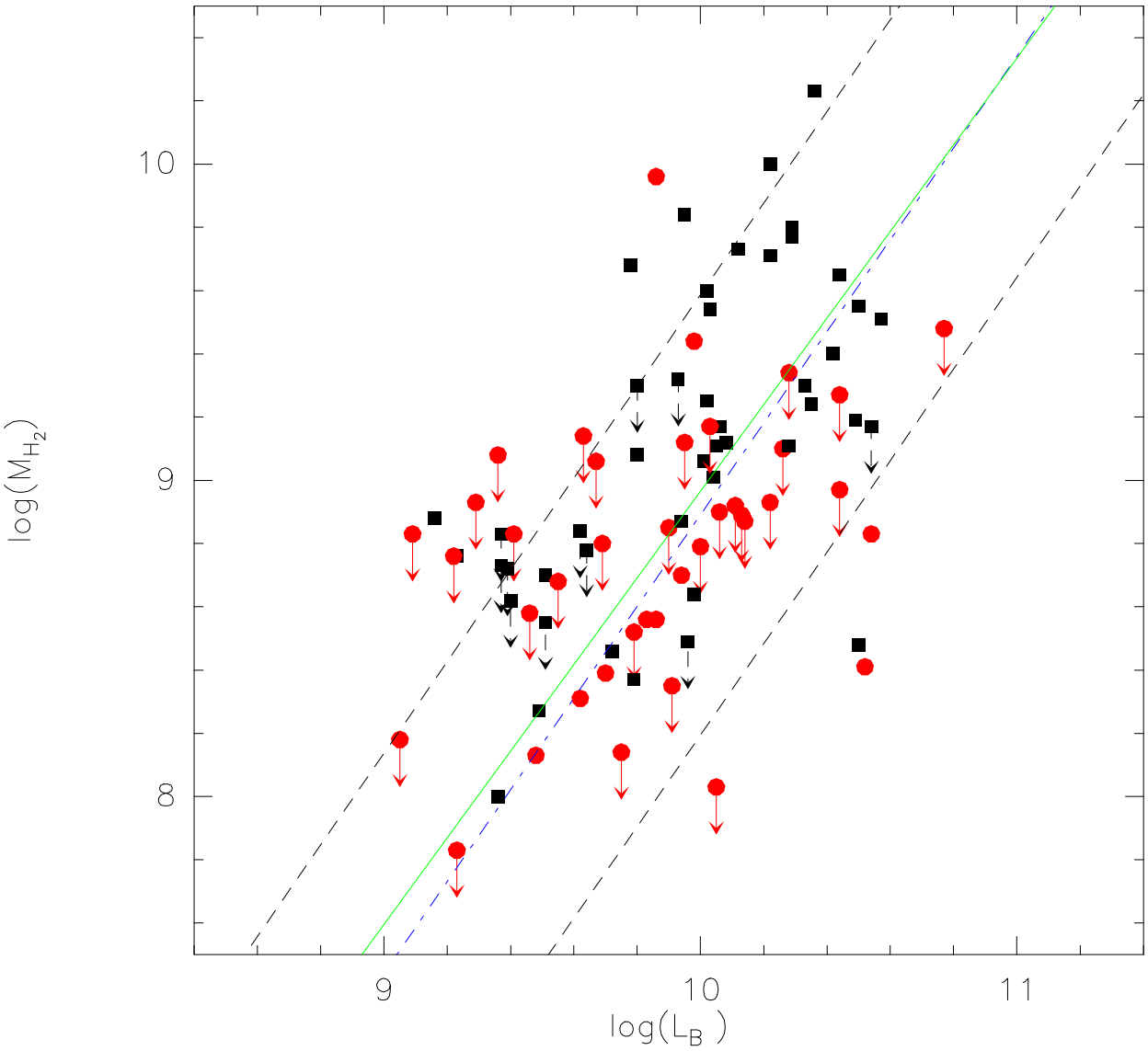
10
9
8
log(M_H2)
9
10
11
log(L_B)

a)
10
9
8
log(M_H2)

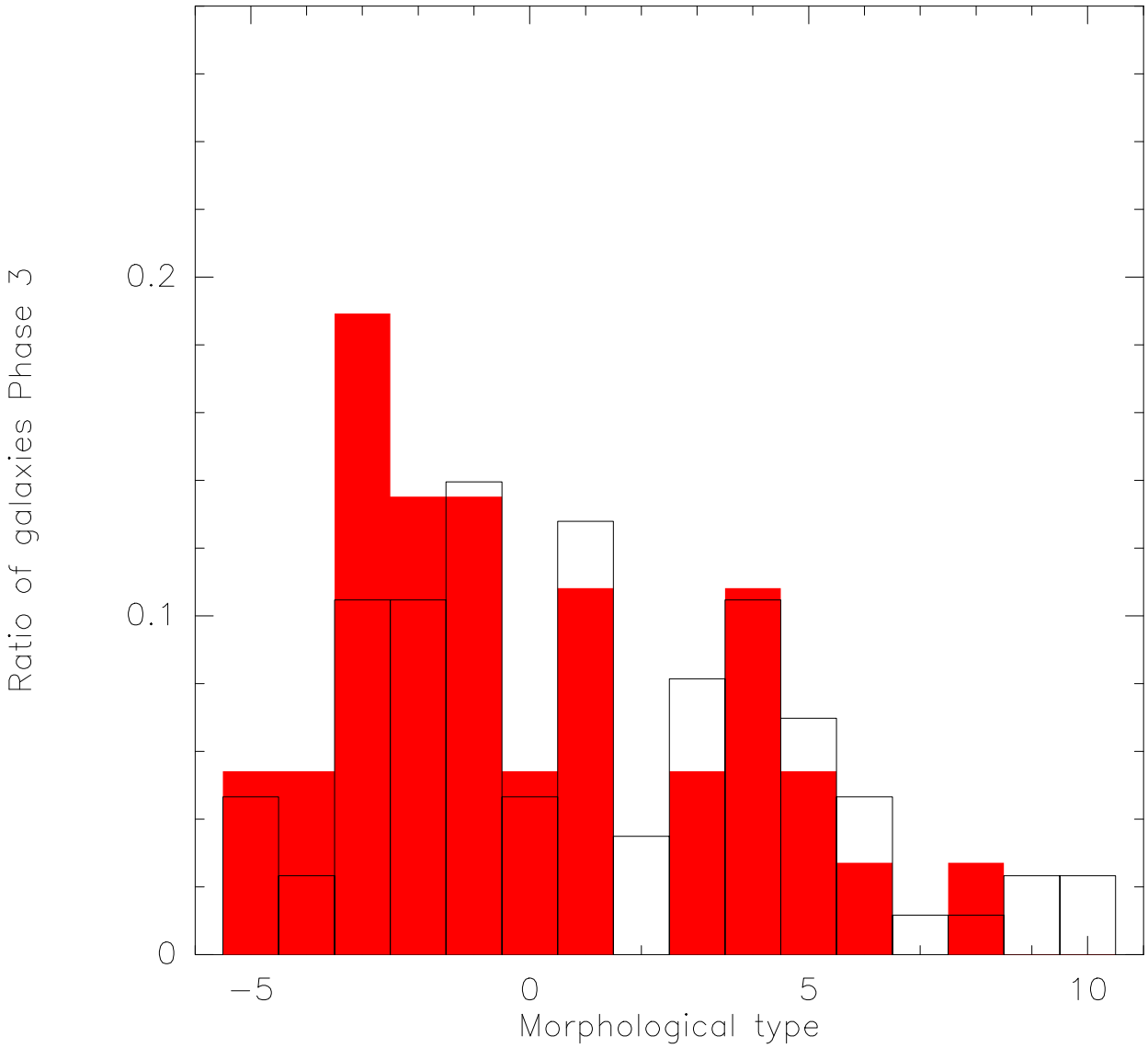
Ratio of galaxies Phase 3
0.2
0.1
0
−5
0
5
10
Morphological type

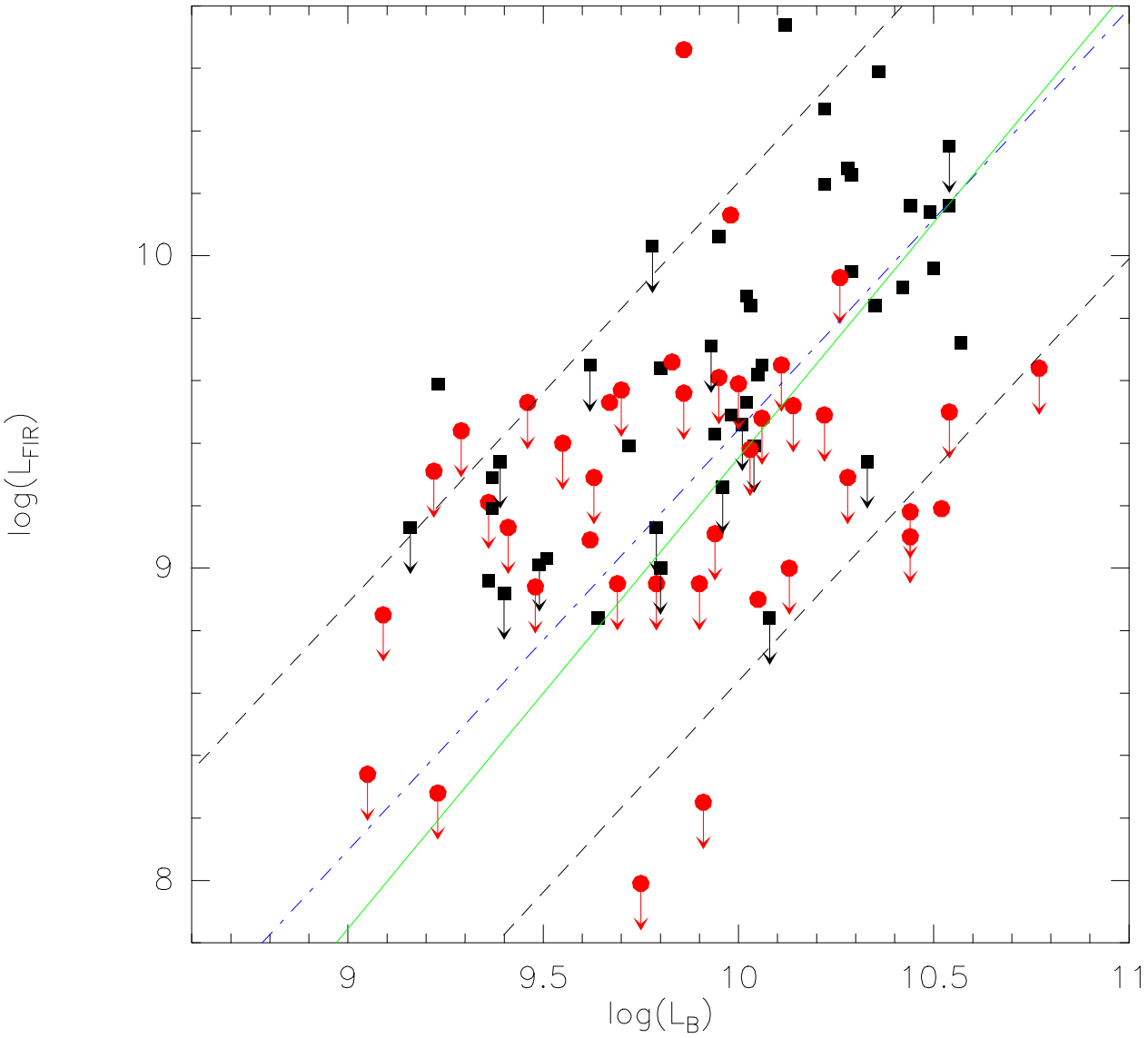
10
9
8
log(L_FIR)
9
9.5
10
10.5
11
log(L_B)

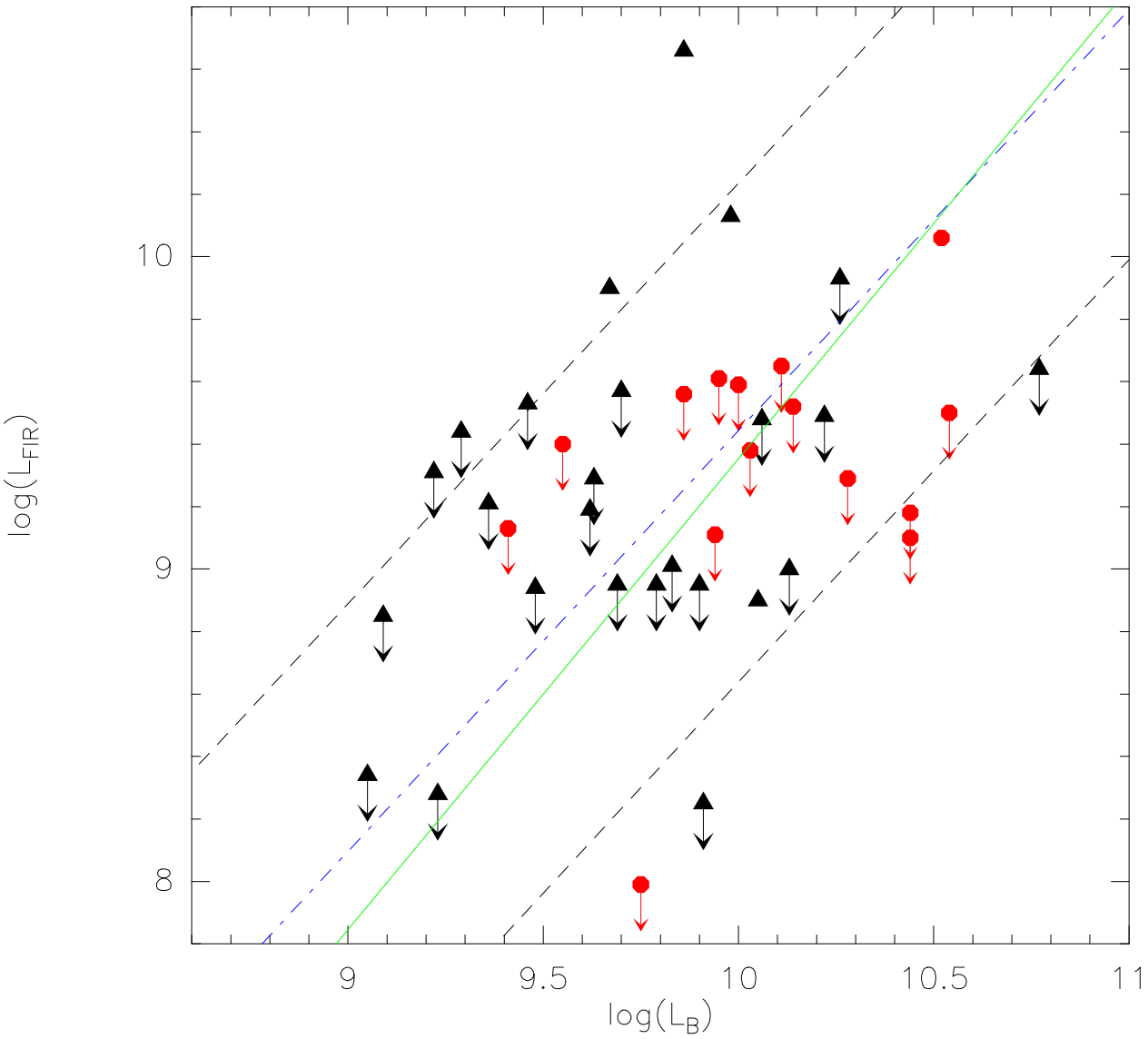
10
9
8
log(L_FIR)
9
9.5
10
10.5
11
log(L_B)

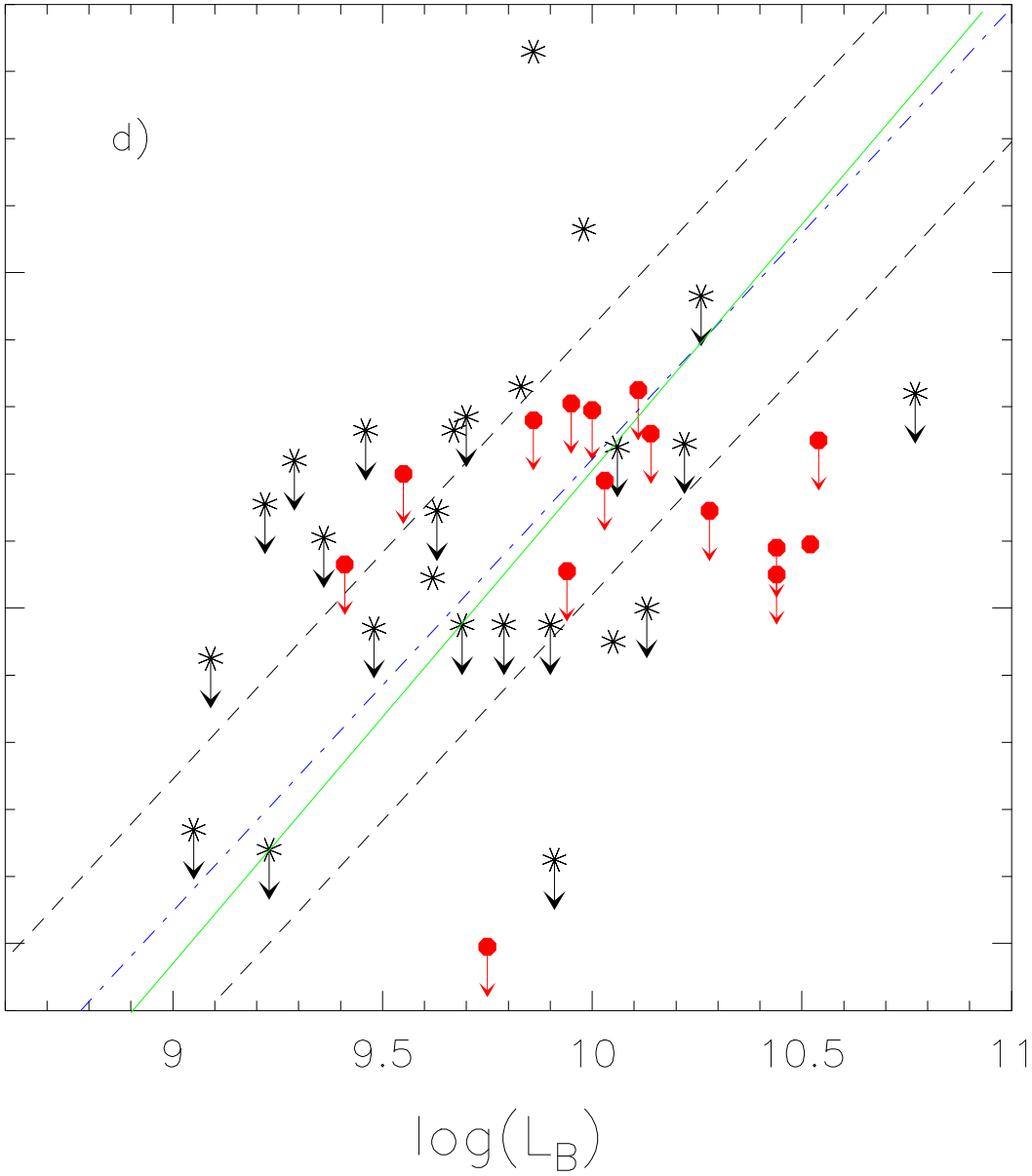
d)
9
9.5
10
10.5
11
log(L_B)

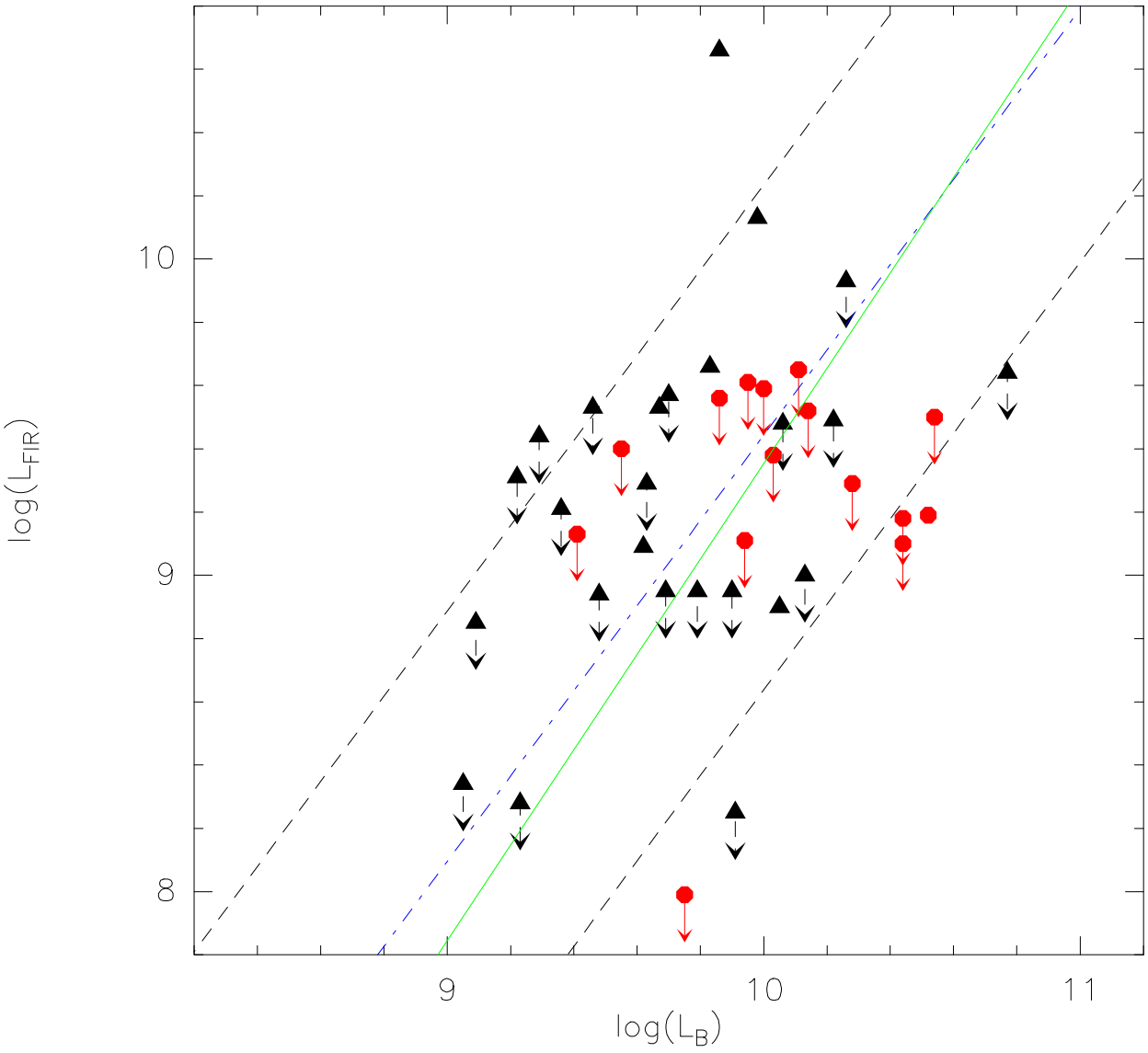
10
9
8
log(L_FIR)
9
10
11
log(L_B)

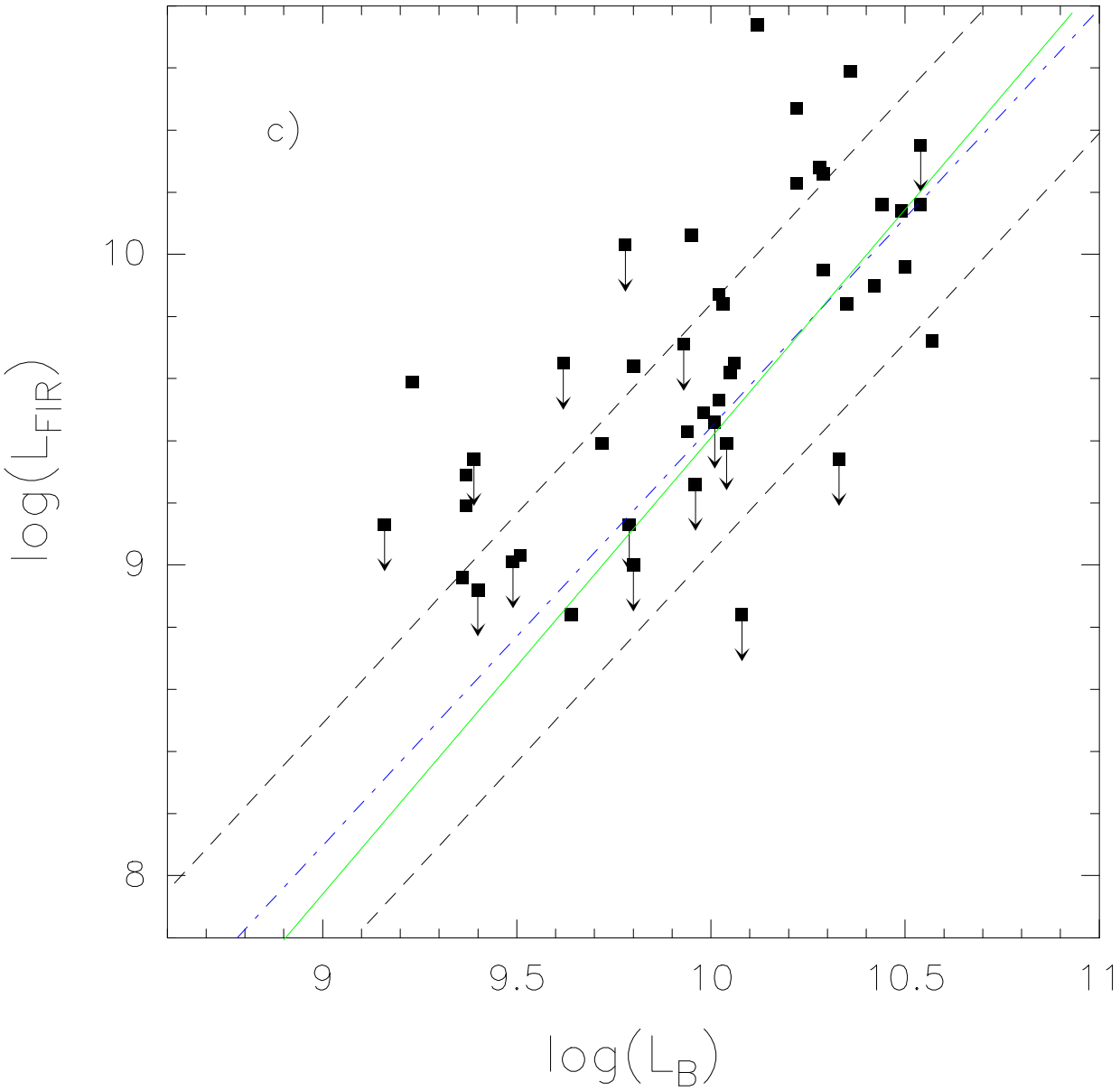
c)
10
9
8
log(L_FIR)
9
9.5
10
10.5
11
log(L_B)

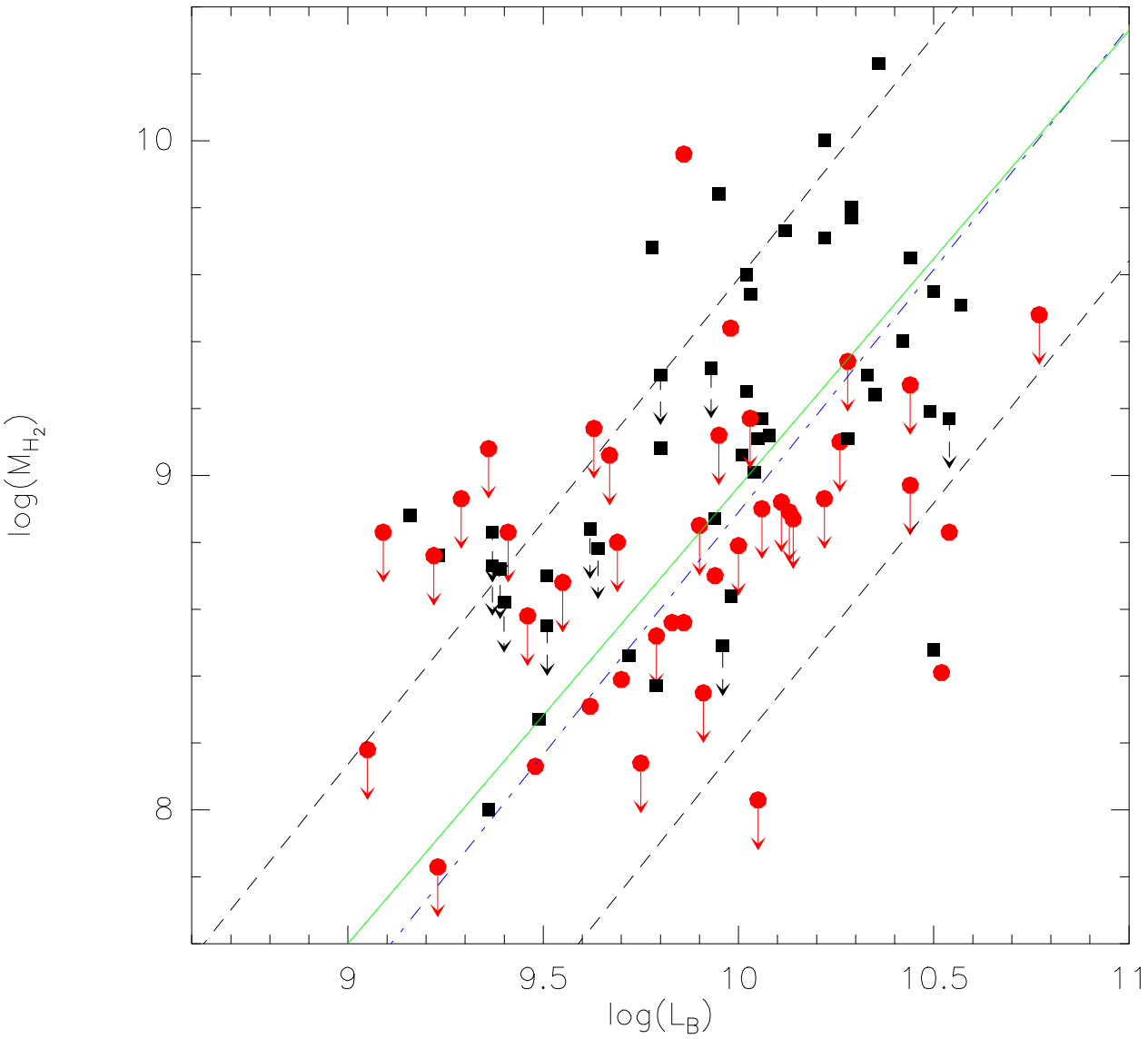
10
9
8
log(M_H2)
9
9.5
10
10.5
11
log(L_B)

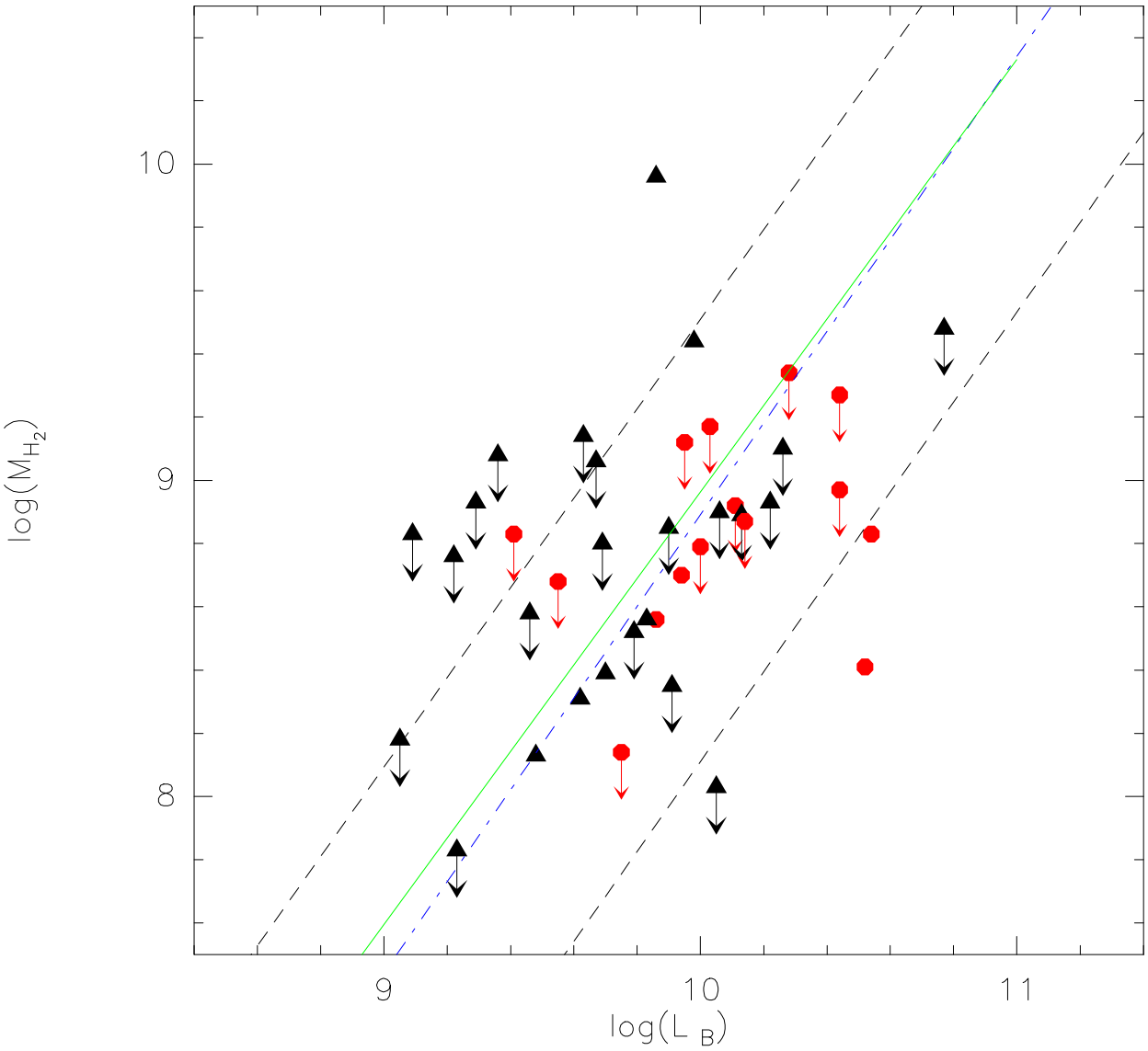
10
9
8
log(M_H2)
9
10
11
log(L_B)

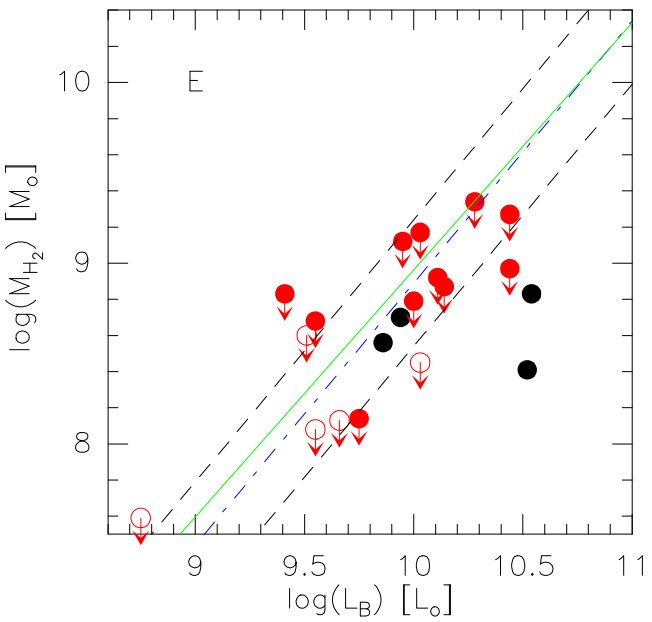
E
10
9
8
9
9.5
10
10.5
11
log(M_H2) [M_o]
log(L_B) [L_o]

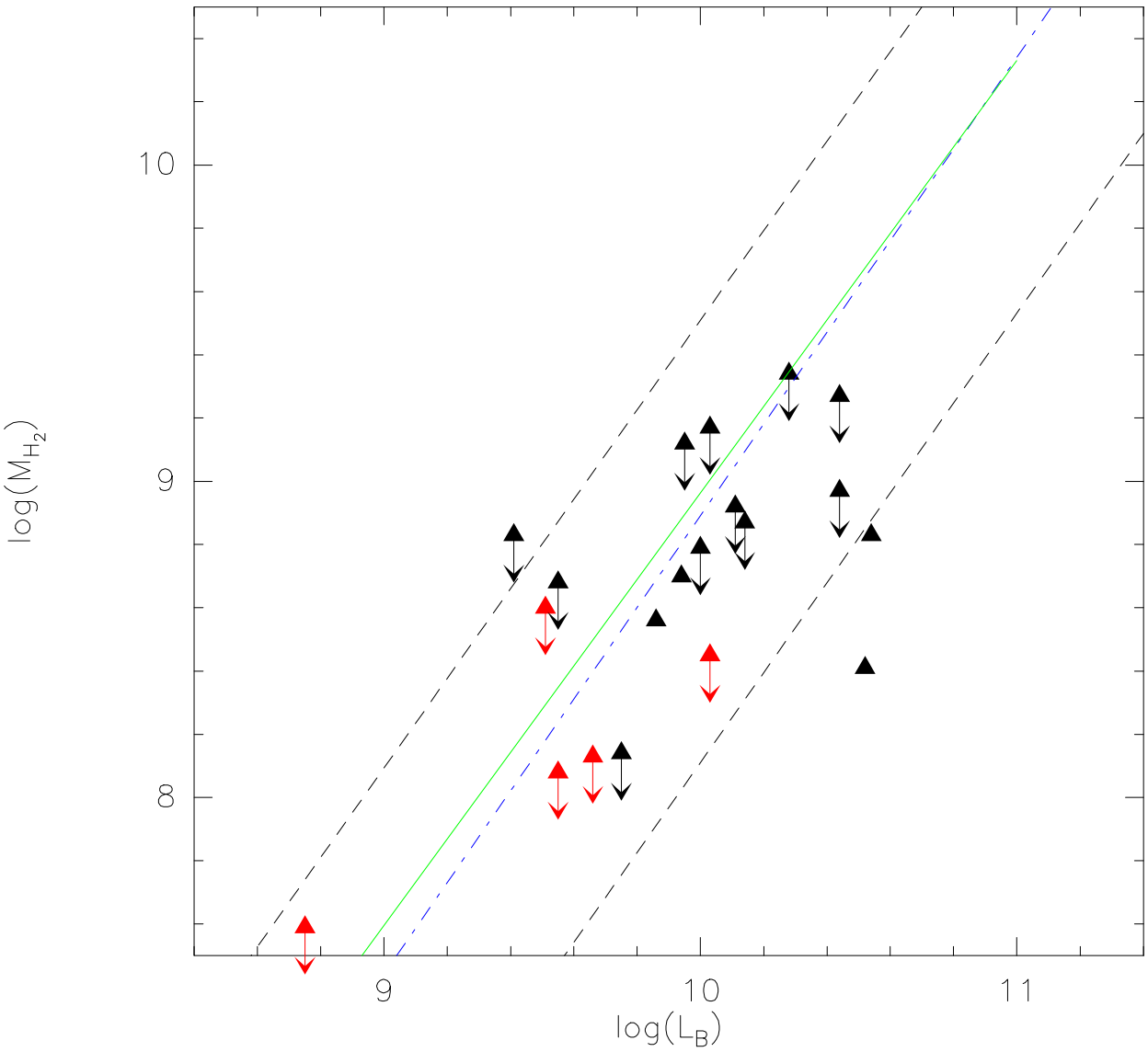
10
9
8
log(M_H2)
9
10
11
log(L_B)